SERBANESCU, RUXANDRA, M.S. *In Silico* Refinement of a Computer Model of GPR55, a Cannabinoid Receptor.(2011)
Directed by Dr. Patricia H. Reggio. 60 pp.

Cannabinoid receptors have great therapeutic potential and are important targets in drug discovery. As part of a broader project whose long-term goal is the determination of the basis for the actions of cannabinoids at the molecular level, this research project focuses on increasing the knowledge of the newly discovered third cannabinoid receptor, GPR55, through computer simulations by refining the model of the inactive (R) state of GPR55.

In order to explore the conformational space available to specific transmembrane helices (TMHs) of GPR55, the Conformational Memories (CM), a computational method was used. CM is a Monte Carlo/Simulated Annealing (MC/SA) algorithm that can employ different molecular force fields. In the first part of this work the force field employed and the starting structure used were varied in order to optimize the method. This was done by exploring the conformational space of the second transmembrane helix (TMH2) of CB2, for which experimental data was available for validation.

The GPR55 sequence exhibits many of the key sequence motifs of the Class A GPCRs and can therefore be easily aligned with other Class A GPCR sequences. From this alignment possible flexible regions of amino acids on each helix were identified for exploration. The regions were: VLSLP in TMH2, KVFFP, GFLLP, MGIMG in TMH5, VSFLP in TMH6, and CCLDV in TMH7. The calculated conformational space available to these helices is of special importance when building the computer model of GPR55 so that the resultant model reflects the sequence dictated conformation of the receptor bundle.

At the beginning of this project, rhodopsin (Rho), the prototype receptor of Class A GPCRs, was the only transmembrane protein for which the crystal structure has been solved.

For this reason and because GPR55 has sufficiently sequence similarity with Rho, this receptor was used as a template to build an initial model presented in a poster at the 2006 International Cannabinoid Research Society meeting.

The results revealed differences between the conformational tendencies of GPR55 TMHs compared to the template. In the case of the TMH2 population, most helices reached over towards TMH3 more than rhodopsin, while TMH5 bends away from the template regardless of which flexible region was varied. The results of TMH6 conformational memories showed that this population leaned toward the TMH5 at the extracellular end. The present work deepens our understanding of the structure of GPR55 and the conformational differences between it and Rho that are dictated by divergences in amino acid sequence.

IN SILICO REFINEMENT OF A COMPUTER MODEL OF GPR55, A CANNABINOID RECEPTOR

By

Ruxandra Serbanescu

A Thesis Submitted to
The Faculty of the Graduate School at
The University of North Carolina at Greensboro
In Partial Fulfillment
Of the Requirements for the Degree
Master of Science

Greensboro

2011

Approved by

_____

Committee Chair

APPROVAL PAGE

This thesis has been approved by the following committee of the Faculty of The Graduate School at The University of North Carolina at Greensboro.

Committee Chair_____

Committee Members_____

_____

_____

Date of Acceptance by Committee

_____

Date of Final Oral Examination

TABLE OF CONTENTS

Page

Page

LIST OF TABLES

Page

LIST OF FIGURES

Page

PREFACE

As part of a broader project whose long-term goal is the determination of the basis for the actions of cannabinoids at the molecular level, this research project focuses on increasing the knowledge of the third cannabinoid receptor, GPR55, through computer simulations. Specifically, the work planned here will be used to refine the model of the inactive (R) state of GPR55.

Specific Aim 1: Computational Method Optimization

First the biased MC/SA computational method used to explore the conformational mobility of the receptor's individual helices and described in the RESEARCH AND METHODS section was optimized. Variations in the force field (AMBER* or CHARMM) and in the starting structure employed were compared in the context of a case study about the role that TMH6 of CB2 has in the ligand-receptor activation and in the ligand-independent activation. Relevant experimental data is available for validation.

Specific Aim 2: Refinement of R State Model of GPR55

The initial model of GPR55 reported here in the RESULTS section was based upon a Rho crystal structure template, from the Protein Data Bank (1GZM structure). Reggio and co-workers have studied CB1/CB2 extensively in the last couple of decades and have shown that although the Rho crystal structure is a good starting point for the cannabinoid receptor modeling, there are sequence dictated differences between it and each of the cannabinoid receptors. In the work reported here, the optimized MC/SA CM method was employed to study some of the sequence dictated differences from a Rho template in TMH2, 5, 6 and 7 of the GPR55 receptor.

The conformational space available to these helices due to their flexible region(s) was explored. From experimental data available about GPR55 interactions with other known cannabinoid ligands and from the results obtained, appropriate helix conformations were used in the refinement of an existing R state model of this receptor. In TMH2 the flexible region from V2.54 to P2.58 was considered. Secondly, the conformational space allowed by possibly three regions of flexibility in TMH5 was explored. These regions are: K5.37-P5.41, G5.46-P5.50, and M5.51-G5.55. In TMH6 the region from V6.46 to P6.50 was examined while in TMH7 the region between C7.46 to V7.50. These studies should contribute to an increased understanding of the actions of cannabinoids at a molecular level.

CHAPTER I

INTRODUCTION

1.1 Membrane Protein Structure Determination

Because membrane proteins have key biological functions such as ion transport and regulation, energy transduction, molecular recognition and response, they are major targets for many pharmacological compounds. Therefore, determining the structure of these proteins and the conformational changes that occur during activation would be invaluable for developments in drug design. For example, after the structure is determined, site-directed mutagenesis can be used to change specific aspects of the architecture of the molecule and study the resulting molecular structure change and correlate it with the degree of functional change.

Mammalian cell membranes are complex mixtures of different lipids and proteins. The lipids interact with one another to form bilayers, and the proteins span the bilayers or bind to the outer surfaces. Almost a quarter of the genes in most genomes encode membrane proteins (Yeagle and Albert 2007) and 30 percent of proteins expressed in eukaryotic cells are supposed to be membrane proteins (Thomas 2001). However, in spite of the increasing number of solved protein structures, most of them are globular proteins and very few are integral membrane proteins (Yeagle and Albert 2007). Membrane proteins are much more difficult to study than soluble proteins, due to the physiochemical properties that they must have in order to exist in the

hydrophobic environment of the lipid bilayer and the hydrophilic extra-membrane regions. Because of their amphipathic nature, these proteins are not soluble in aqueous solutions. The majority of the methods existing today for the analysis of proteins are designed for water-soluble proteins. Some of these methods include 2D polyacrylamide gel (PAGE) electrophoresis, capillary electrophoresis, chromatography, electron microscopy, atomic force microscopy (Engel and Muller 2000), matrix-assisted laser desorption/ionization (MALDI) electrospray mass spectrometry, 2D NMR (Thomas 2001) and X-ray crystallography. Another crystallographic method, high resolution X-ray powder diffraction has also been used in the last decade to solve and refine protein structure (Von Dreele 1999; Von Dreele, Stephens et al. 2000). Membrane proteins denature outside the membrane therefore, adaptations of these techniques to membrane proteins have been met with only limited success. Detergents, which mimic the lipid bilayer, are used in order to solubilize membrane proteins in aqueous environments. However, the use of detergents inhibits their crystallization and decreases the resolution significantly in X-ray crystallography, for example. The resolution is a global measure of the model quality and ranges from low resolution, in which case only the general shape of the protein is revealed, to high resolution (1-2 Å), where most atomic positions can be detected. Uncertainty may still be present even in the structures obtained at very high resolution due to the inherent mobility of amino acid side chains. The most dynamic side chains will give variations in conformations that cause unclear images, which could be a valuable indication of where the most mobile regions are located.

In spite of the numerous obstacles that membrane proteins present when attempting to crystallize them, a variety of different protein modification and engineering approaches have contributed to recent advances in GPCR crystallography. To date there are four inactive-state crystal structures of four GPCRs for comparison: the human beta 2 adrenergic (β2-AR) receptor

bound to the high affinity inverse agonists carazolol and timolol (Rasmussen, Choi et al. 2007) acian beta 1 adrenergic (β1-AR) receptor bound to the antagonist cyanopindolol (Warne, Serrano-Vega et al. 2008) the human A_{2A} adenosine receptor bound to the antagonist ZM241385 (Jaakola, Griffith et al. 2008) and bovine rhodopsin containing the covalently bound inverse agonist 11-*cis* retinal (Palczewski, Kumasaka et al. 2000).

Many GPCRs exhibit constitutive activity (CA), which is inhibited by inverse agonists or antagonists. Constitutive activity is the biological response that is produced by receptors in the absence of ligand. These ligands stabilize the ground state of the protein significantly, improving the chances of its crystallization. For this reason and to gain information about the binding site and its interaction with a ligand, the protein is often bound to an antagonist or inverse agonist and stabilized in an inactive state. This can increase the thermal stability enough that a greater variety of crystallization conditions may be allowed. Unlike rhodopsin, most GPCR's have poor thermal stability and are subject to proteolysis due to the presence of their disordered loops that extend outside the membrane. Thermodynamic and proteolytic protein stability problems have been overcome by implementing mutations in the β1-AR receptor crystallization (Jaakola, Griffith et al. 2008), or by adding lipids during purification and crystallization in order to stabilize mobile regions of the protein and to create an environment more like the natural one. Often cholesterol or other lipids were added during the rhodopsin crystallization and during the more recent crystallization of the beta-2-adrenergic with or without lysozyme T4L, and of the adenosine A_{2A} coupled to T4L (Jaakola, Griffith et al. 2008). In other instances, high salt concentration improved the thermal stability such as in the case of the adenosine A_{2A} receptor crystallization. In order to enhance the proteolytic stability, at times truncation of the disordered regions has been employed, especially around the C-terminus, or of certain amino acids such serine, threonine

phosphorylation sites, or N-linked glycosilation sites since most post-translational modifications can be very heterogeneous (Cherezov, Rosenbaum et al. 2007; Hanson, Cherezov et al. 2008; Jaakola, Griffith et al. 2008). Another method used towards achieving stability has been the complex formation with antibody Fab fragment as was performed in the case of the beta-2-adrenergic and adenosine A_{2A} crystallization (Rasmussen, Choi et al. 2007). A common problem that had to be overcome is the fact that, in native tissues, most of these receptors (with the notable exception of rhodopsin) are expressed only at very low levels and therefore a suitable recombinant expression system usually has to be developed in order to generate membrane proteins that are folded properly.

Computer simulation and modeling methods have the potential to complement experimental investigations and make a great contribution to the studies of protein structure (Mulholland, Grant et al. 1993; Mulholland and Karplus 1996). Using experimental structural information as a starting point, calculations can be performed in order to address questions that may be quite difficult or impossible to approach by experiment alone. For example, often proteins are mutated in order to enhance their wild type stability (Park, Scheerer et al. 2008; Warne, Serrano-Vega et al. 2008) but computer simulations do not require such mutations.

Numerous computational molecular modeling methods are available, ranging from quantum chemistry to the interpretation of three-dimensional structure. All techniques have certain strengths and weaknesses depending on the systems for which they were designed, so it is necessary to choose an appropriate method for the particular type of problem under investigation.

1.2 Molecular Modeling Method

The availability of powerful and relatively inexpensive computers has revolutionized science by allowing computer simulations to be used as one of the most versatile and capable tools. Such computer calculations are now employed to create relevant models, to explain observed phenomena, to predict verifiable results, to explore possibilities, and to help develop answers as well as questions. In the work presented here, the conformational space available to specific transmembrane helices (TMHs) of cannabinoid (CB) receptors was explored using Conformational Memories (CM) (Guarnieri and Wilson 1995; Guarnieri and Weinstein 1996), a Monte Carlo/simulated annealing (MC/SA) algorithm employing either the AMBER* (Weiner, Kollman et al. 1984) or CHARMM force field (Brooks, Bruccoleri et al. 1983). CM is a stochastic and nonsystematic method meaning that the sampling is random in nature and uses statistical approaches which typically make it better suited for larger biomolecules (Chang, Guida et al. 2002; Ferguson and Raber 2002).

The random nature of a Monte Carlo simulation assures that in the long run the simulation approaches equilibrium values, while an individual move has a real chance of moving the simulation away from equilibrium. What follows is a discussion of the theory behind the molecular mechanics calculation, including a description of the conformational memories method, geometry optimization method, and the force field parameters. The actual experimental set up is presented in the RESEARCH AND DESIGN METHODS section.

1.2.1 Conformational Memories (MC/SA algorithm)

In general, an annealing process consists of three stages: heating to a desired temperature, holding that temperature, and 'annealing' or slow 'cooling' plan, usually to either biological or room temperature. Such an annealing process can be modeled successfully by computer simulation methods that use the Metropolis Monte Carlo algorithm proposed in 1953 (Metropolis, Rosenbluth et al. 1953). In short, the Metropolis Monte Carlo Algorithm performs an "annealing": at high temperatures, with 90% of all new conformations typically "accepted". An opposite trend starts to happen as the system is slowly cooled, until, at low temperatures, 90% of all new conformations are "rejected". The Metropolis Monte Carlo algorithm, also known as the Boltzmann-Weighted Monte Carlo algorithm is an acceptance criterion used to determine if a new conformation is added or not to the ensemble. This criterion minimizes the possibility of unrealistic samples being considered. The energy of each new conformation is evaluated and if it is less than the energy of the old conformation, then that conformation is kept. If the energy is higher though, the Boltzmann probability of that conformation to occur at the current temperature is calculated. This probability is a number between 0 and 1 and is compared to a random number between 0 and 1. If the Boltzmann probability is higher than the random number, then the conformation of higher energy is kept. The willingness to move uphill to a worse position gives simulated annealing the advantage of possibly escaping from local minima in hope of finding a deeper valley farther away, which prevents the simulation from becoming stuck in a valley that cannot be escaped by taking only downhill moves. In that sense, temperature is the control parameter that represents the willingness to accept a bad move. When the value of the temperature is large the willingness is great. If the probability is lower than the random number, then the move is not accepted and the previous state is restored. After a certain number of moves,

the temperature is decreased. The Metropolis Monte Carlo simulation is then continued. This process is repeated until the final temperature is reached. Two cooling schedules are most frequently reported in the literature: linear or proportional. In the experiments conducted here the proportional cooling schedule employed obeyed $T_{new} = 0.8995 \times T_{old.}$ When no downhill (better) moves exist in the neighborhood, a local minimum has been reached. This does not imply that it is the global minimum, however. The algorithm terminates when some specified stopping criterion is met (for example when no improvement has been found for some number of moves). The factors that control how thoroughly the space of the system is searched are the size of each Monte Carlo step and the number N of the steps attempted. Also, by using this acceptance probability criterion one can prove that the average of any property, such as energy, over the ensemble is equal to the Boltzmann average of this property as determined by the Boltzmann Distribution Law for a sufficiently large ensemble. The Boltzmann average of a property is the expected value of this property at the given temperature (Metropolis, Rosenbluth et al. 1953; Kirkpatrick 1983).

Monte Carlo methods require very long samplings due to the fact that statistical methods require more steps for completeness. In order to prove that the MC search has sampled long enough, the simulation should converge to the same ensemble regardless of the starting conformation, seed number (the "kick" or velocity given to move atom coordinates in a random direction), cooling schedule, or initial and final effective temperatures. In practical terms, the number of steps has to be computationally reasonable, and often some dependence of these parameters on the final result does exist.

Thus, the most difficult aspect of the MC/SA is to determine how long to run the simulation at each temperature. While the simulation attempts to reproduce the correct

Figure 1. A quick schematic of the Metropolis Monte Carlo algorithm.

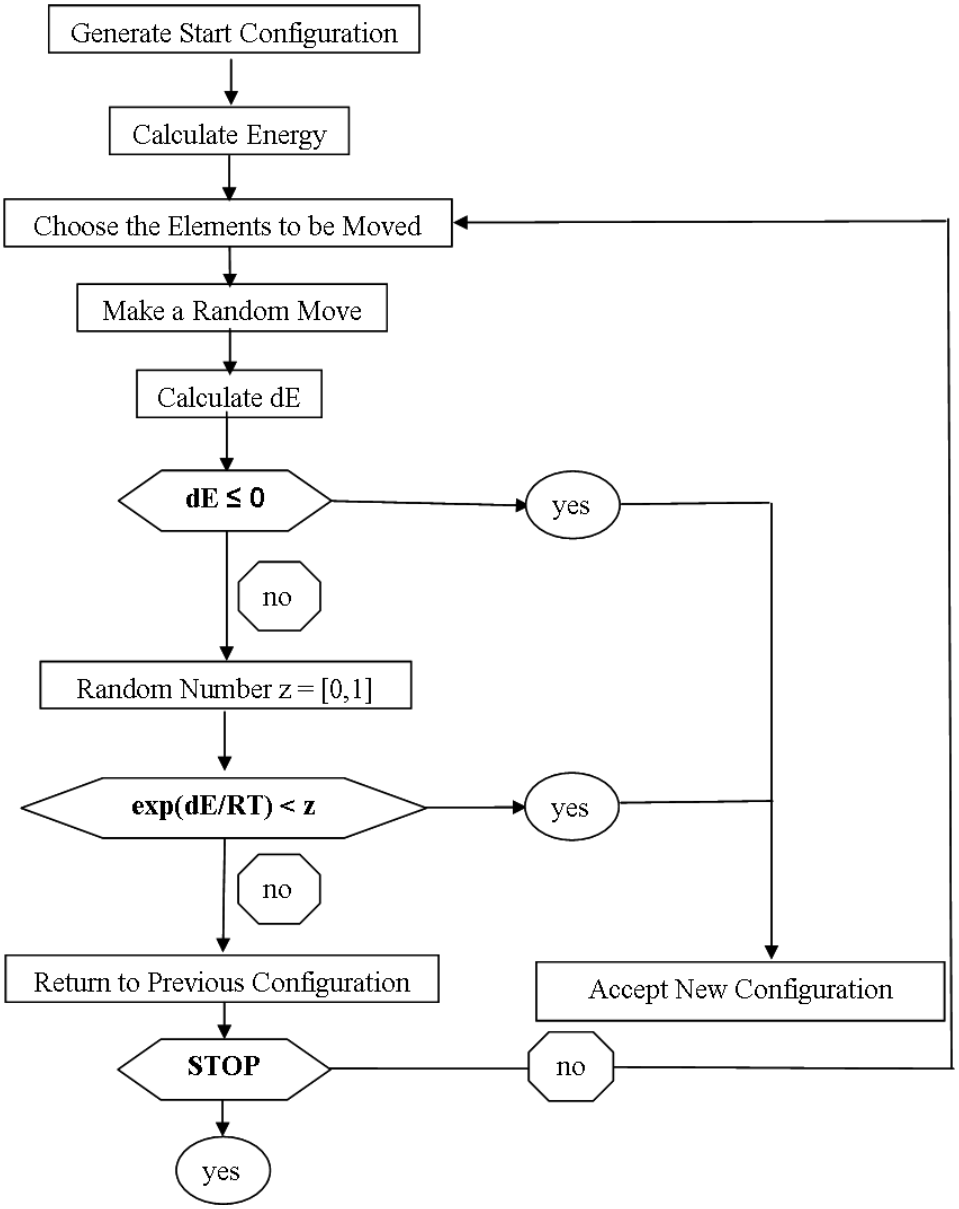

Boltzmann distribution at a given temperature, it only needs to run long enough to explore the regions of search space that should be reasonably populated. This allows for a reduction in the number of MC steps at each temperature, but the balance between the maximum step size and the

number of Monte Carlo steps is often difficult to achieve, and depends very much on the characteristics of the search space or the energy landscape. In general, temperature is used to scale differences in height of the landscape. Raising the temperature flattens a rugged landscape by a greater willingness to accept worse moves. Small irregularities on a smooth landscape are accentuated by lowering the temperature and accepting mostly improving moves (Metropolis, Rosenbluth et al. 1953).

In short, the Monte Carlo algorithm starts out at a temperature of 2070K and the energy of the current conformation evaluated. The atomic coordinates are then moved in a random direction and the energy of the new conformation is compared to the original conformation. If this energy is smaller the new conformation is kept and if it is higher, the Boltzman probability, ($P = e^{-(\varepsilon 1 - \varepsilon 0)/kT}$) is compared to a random number, R, between 0 and 1 and the new conformation is kept only if P is greater than R. These steps are repeated as many times as possible while the temperature follows a proportional cooling schedule according to $T_{new} = 0.9 * T_{old}$ for 19 temperatures from $T_{start} = 2070$ K to $T_{final} = 310$ K.

1.2.2 Force Fields (AMBER*, CHARMM)

The first calculations based on force field methods were reported back in 1946 (Ponder and Case 2003) and were known as the *Westheimer methods* but they did not become more developed until the 1970s because of the increased availability of computers. They are based on classical mechanics laws and use the ball-and-stick model for approximation of molecules. The total energy of a molecule is assumed to be the sum of the individual energy components such as the intramolecular or internal, bonded terms (bond-stretching, angle-bending, torsional terms, impropers, Urey-Bradley) and intermolecular or external, nonbonded terms (van der Waals or electrostatic), as functions of conformations.

The force fields used in molecular modeling have to reproduce structural properties. Force fields that have identical functional form may still have very different parameters. Empirical 'molecular mechanics' potential functions have been developed that can model protein structure and dynamics effectively and efficiently. Potential functions or force fields are mathematical functions that return energy as a function of conformation. Many force fields used for modeling proteins and other biological macromolecules are sums of terms that correspond to bond, angle, torsion angle, van der Waals, and electrostatic interaction energies as functions of conformation. Equation #1 below, illustrates the basic form of the force fields used for modeling proteins and other biological macromolecules.

$$V(r) = \sum_{\text{bonds}} \frac{k_r}{2}(r - r_0)^2 + \sum_{\text{bond angles}} \frac{k_\theta}{2}(\theta - \theta_0)^2 + \\ + \sum_{\text{torsion angles}} [\mathrm{k}_\phi(1 + \cos(n\phi - \delta)]^2 + \sum_{\text{atom pairs}} \frac{q_i q_j}{r_{ij}} + \frac{A_{ij}}{r^{12}{}_{ij}} - \frac{C_{ij}}{r^{6}{}_{ij}} \qquad \text{(eq. \#1)}$$

In the above expression kr and k_θ are force constants in harmonic potentials for bonds and angles with equilibrium values r_0 and θ_0 and actual values r and θ respectively. Cosine functions are usually used for the potential associated with torsion angle variation, with the multiplicity of the function n between 1 and 5 and the phase angle δ. A Lennard-Jones (12, 6) potential is used for attractive dispersion (with coefficient C_{ij}) and close range repulsion (with coefficient A_{ij}) non-bonded interactions, where r_{ij} is the distance between non-bonded atoms q_i and q_j. The electrostatic interactions between non-bonded atoms depend on the atomic partial charges q_i and q_j. To reduce the computational expense of a simulation, the number of non-bonded interactions can be limited by applying a cut-off beyond which no interactions are calculated. A cut-off range

is applied after which no van der Waals energies are calculated, this is normally between 8 and 12 Å. The cut-off is often used with a 'switching function', which multiplies the van der Waals interactions and causes it to go smoothly to zero at the cut-off distance.

Figure 2. Energy components illustration.

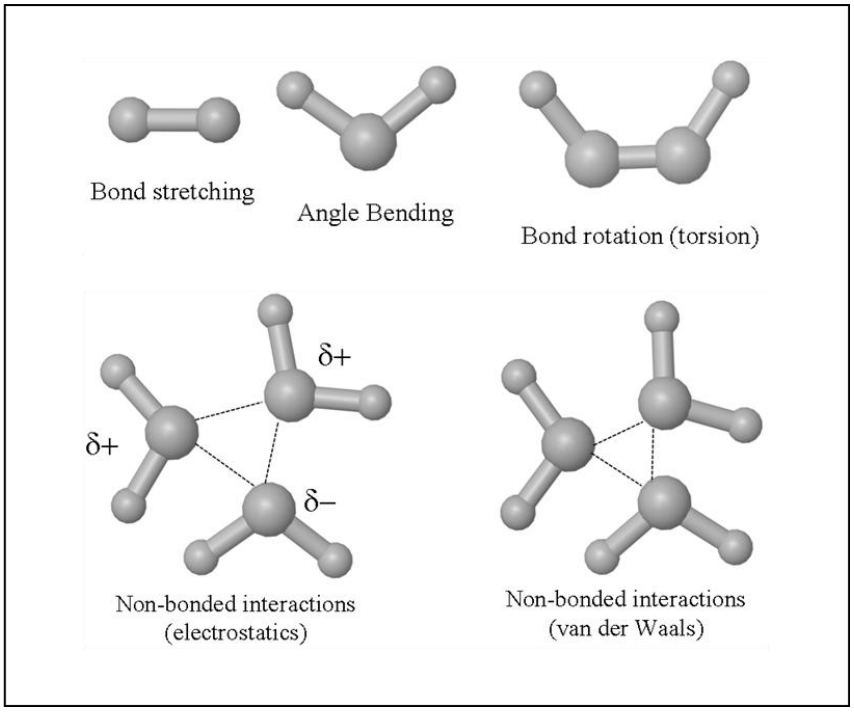

Due to their low computational expense molecular mechanics force fields can handle long dynamics simulations of entire solvated proteins (Ponder and Case 2003). In addition to the functional form of the potentials, force fields also define parameters for individual types of atoms, and distinct parameters for individual type of atoms in different environments such as oxygen in a carbonyl versus a hydroxyl. Again, the parameters from one force field should not be used in combination with the parameters from a different force field, regardless of how closely related, because they may vary extensively.

1.2.3 Geometry Optimization

It is difficult to locate the minimum on a potential energy surface analytically, due to its complex nature. Instead, numerical methods are used which gradually change the coordinates in the direction of decreasing energy until a minimum is reached. Most minimization algorithms achieve this by using derivatives. It is useful to write the potential energy function of a system as a Taylor expansion: for a continuous differentiable function in one dimension at the point x, this is given in terms of the function and its derivatives at the point x_0.

$$V(x) = V(x_0) + (x - x_0)V'(x_0) + \tfrac{1}{2}(x - x_0)^2 V''(x_0) + \ldots \qquad \text{(eq. \#2)}$$

For a non-linear molecule, the energy is a function of $3N$ Cartesian coordinates (or $3N$ - 6 internal coordinates), and so the equivalent multidimensional expression from equation # 2 applies. In this multidimensional function x is replaced by the vector $\boldsymbol{x}$ and matrices are used for the derivatives.

There are many methods that have been developed for molecular energy minimization and these are classified according to the highest-order derivative they use. The first order methods use only the gradient of the function, e.g. steepest descent (Wiberg 2002) and the Powell conjugate gradient (Fletcher and Powell 1963), whereas second order methods use both the first and second derivatives, e.g. adopted basis Newton-Raphson (Boyd 1968). In this work, steepest descent minimizations have been used.

1.2.3.a Steepest Descent

Steepest descent is a simple minimization method where each step involves moving in a negative direction to the gradient (Wiberg 2002). At every iteration, if the step decreases the energy, the size of the next step is increased, whereas if the energy is increased, the step size is decreased. Steepest descent minimization is widely used in studies of biomolecules. Its main advantage is that the energy can be lowered very quickly. The disadvantage is that as the minimum is approached, the rate of convergence slows down and the minimum may never be reached. In practice, steepest descent is used at the beginning of minimization protocols, to relieve bad non-bonded contacts or reduce strain in a system.

1.2.4 Dielectric Constant

The dielectric constant basically dampens the charge-charge interactions and is a function of the solvent. The greater the value, the less electrostatic interactions exist between the atom pair. For example, in a vacuum the dielectric constant is 1.0, in water ~80, in lipid 3-5. The charges can be used from a file or from a force field (for example, in AMBER, a popular way to generate an electrostatic potential is from high level *ab initio* calculations and then fit the optimal point charge distribution on the atoms via least-squares methods).

1.3 Historical Overview of the Cannabinoid System

Cannabis sativa, the plant from which Δ^9-tetrahydrocannabinol (THC) is derived, is still one of the most abused drugs in the world. It wasn't until the 1960's that the structure of the principal psychoactive compound present in the plant (Δ^9-THC) was elucidated and later some of the specific effects of this compound could only be explained if they were due to action on

receptors or enzymes. In 1988, Allyn Howlett and her group (Devane, Dysarz et al. 1988) showed that there is a cannabinoid receptor (CB1) in the brain. Subsequently, since nature would not have designed receptors just for the sole purpose of binding plant-derived compounds, researchers looked for endogenous cannabinoid ligands. In the 1990's, anandamide (AEA) (Devane, Hanus et al. 1992) and 2-arachidonoyl glycerol (2-AG) (Mechoulam, Ben-Shabat et al. 1995) were found as the natural ligands produced by the body for interaction with cannabinoid receptors. A second cannabinoid (CB2) receptor was also identified in the spleen (Munro, Thomas et al. 1993). Additionally, endogenous cannabinoids are found present in mammalian cells early in their development, as well as in some of the simplest multicellular organisms. This suggests a basic and vital role that the cannabinoid system plays in the biology of these organisms, including humans.

In the last couple of decades there has been an increased interest in the potential medicinal properties of the cannabinoids and their possible role in modulating neurobiological activities. This is due to the fact that the endocannabinoid system appears to play a role in a large number of physiological processes, including nervous functions, emotions, movement, learning, memory, pain, appetite, blood and intraocular pressure, regulation of cell development and growth, and immune and reproductive functions (Goutopoulos and Makriyannis 2002). Most of these effects have been attributed to action at either the cannabinoid CB1 or CB2 receptors that are found in most biological systems. However, some cannabinoid effects are not due to action at either CB1 or CB2. There is quite enough evidence that suggests that some of these cannabinoid effects may be due to the involvement of the endogenous ligand of vanilloid type (TRPV1) receptor and at least one other G protein coupled receptor (GPCR), defined pharmacologically as a cannabinoid receptor only recently: GPR55 (Begg, Pacher et al. 2005). A fairly wide range of

cannabinoid ligands have been reported to display affinity/ efficacy (Brown and Wise 2001; Brown 2007) for GPR55.

1.3.1 G-protein Coupled Receptors (GPCRs) Class A

1.3.1.a GPCRs General Structure

G protein-coupled receptors (GPCRs) represent the largest super-family of the integral transmembrane proteins class. GPCRs are important in activating cellular signal transduction mechanisms; hence they are significant in many vital physiological events. Not surprisingly, GPCRs are major targets for drug development. Because integral proteins are inherently very difficult to crystallize, until 2007 only the Class A GPCR rhodopsin was crystallized (Palczewski, Kumasaka et al. 2000; Teller, Okada et al. 2001; Okada 2002; Li, Edwards et al. 2004; Okada, Sugihara et al. 2004; Nakamichi and Okada 2006; Nakamichi and Okada 2006; Salom, Lodowski et al. 2006). From these Rhodopsin crystal structures, the general topology of G-protein coupled receptors in general, began to be shaped (see Figure 3). GPCR's have an extracellular N terminus, seven transmembrane (TM) alpha helices connected by loops that extend intracellularly and extracellularly and an intracellular C terminus that begins with a short helical segment that runs parallel to the membrane (Helix 8). The availability of the newer crystal structures of the β_2-adrenergic (β_2-AR) (Cherezov, Rosenbaum et al. 2007; Rasmussen, Choi et al. 2007), β_1-adrenergic (β_1-AR) (Serrano-Vega, Magnani et al. 2008), opsin (Park, Scheerer et al. 2008; Scheerer, Park et al. 2008), and adenosine A_{2A} (Jaakola, Griffith et al. 2008), along with the availability of biophysical data on the conformational changes that occur when these receptors are

activated have greatly aided understanding of structure-function relationships of other Class A GPCRs.

Figure 3. Typical GPCR topology.

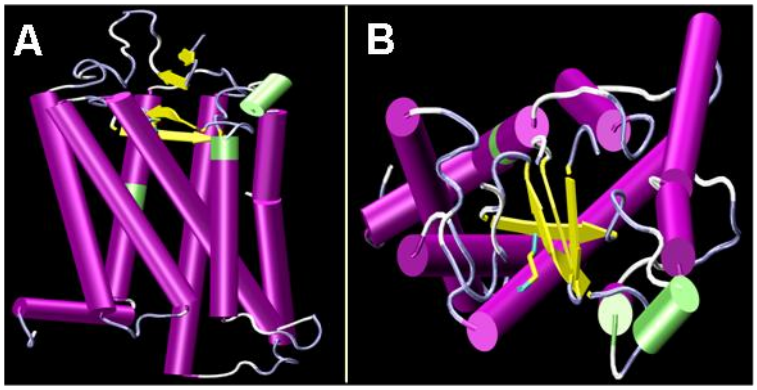

In Figure 3 A the GPCR transmembrane helix bundle is seen from the lipid side in which the N-terminus is at the top of the figure and the C-terminus at the bottom of the figure. Figure 3 B shows the bundle from the extracellular view.

1.3.1.b GPCRs Activation

Most of the in depth information about the conformational changes that may occur when GPCRs become activated has been generated from biophysical studies on these changes in Rho or the β_2-AR. Much evidence has emerged from these studies that suggest activation in these receptors is accompanied by a few movements of key structural domain contacts. These key motifs may be identical in some receptors, but also mimicked by alternate similar domains that form or break and thus promote activation in other receptors (Ballesteros, Shi et al. 2001).

The conventional model of agonist activation of the GPCRs involves two states, a ground or inactive (R) state and an active (R*) state, that are in equilibrium with each other. From studies performed on Rho and the β_2-AR, activation in these receptors is thought to be associated

with the movement of TMH3 and TMH6. P6.50 in TMH6 is part of the highly conserved CWXP motif that may act as a flexible hinge that allows TMH6 to straighten during activation, moving its intracellular end away from the core of the receptor and upwards towards lipid (Jensen, Guarnieri et al. 2001). In Figure 5, the TMH6 sequence of Rho and CB receptors is illustrated. From here it can be seen that in CB receptors, the CWXP amino acid motif is CWGP for CB1, CWFP for CB, and SFLP for GPR55, while in Rho, this motif is CWVP. In the χ_1 β_2-AR, β_1-AR, and A_{2A} this motif is CWLP. From the 2.80 Å Rho crystal structure (Palczewski, Kumasaka et al. 2000), residue W265 (number of the amino acid in the receptor sequence) undergoes a change in its chi1 torsion angle from *g+* (-60°) to *trans* (180°) when Rho is activated (Lin and Sakmar 1996). This amino acid is also designated the notation W6.48 according to the The Ballesteros-Weinstein numbering system (Ballesteros and Weinstein 1995). This notation and the absolute sequence numbers for the TMH6 in a few GPCR's are described bellow and illustrated in Figure 4 and 5, respectively.

CHAPTER II

RESEARCH AND DESIGN METHODS

2.1 Amino Acid Numbering System

The amino acid numbering scheme proposed by Ballesteros and Weinstein is used here when referring to receptor residues (Ballesteros and Weinstein 1995). In this numbering system, the most highly conserved residue in each transmembrane helix (TMH) is assigned a locant of .50. This number is preceded by the TMH number and is followed in parentheses by the sequence number. All other residues in a TMH are numbered relative to this residue. In this numbering system, for example, the most highly conserved residue in TMH2 of the hGPR55 receptor is D2.50(70). The residue that immediately precedes it is F2.49(69). Residues in the intracellular extension of TMH7 (Hx8) are numbered as if they are part of TMH7 following the literature precedent set by Prioleau and co-workers (Prioleau, Visiers et al. 2002). Sequence numbers used are human GPR55 or CB2 sequence numbers unless otherwise noted.

2.2 Definition of Rotameric State of Chi1(χ_1) Angle

When referring to χ_1 torsion angles or the rotameric state of a residue the nomenclature employed here is the one described by Shi et al(Shi, Liapakis et al. 2002). When the heavy atom at the γ position (atom number 1 in Figure 7) is opposite to the backbone nitrogen when viewed

from the β–carbon (atom number 2) to the α–carbon (atom number 3), the χ_1 is defined to be *trans*. Similarly viewed, when the same heavy atom (1) is opposite to the backbone carbon is defined to be *gauche minus* (g-), while when the same heavy atom γ is opposite to the α–hydrogen is defined to be *gauche plus* (g+). Therefore, the side chain conformations discussed here are categorized g- ($0° < \chi_1 < 120°$), trans ($120° < \chi_1 < 240°$), g+ ($240° < \chi_1 < 360°$) (Singh, Hurst et al. 2002).

Figure 4. Illustration of the W6.48 *g plus* and *trans* conformations.

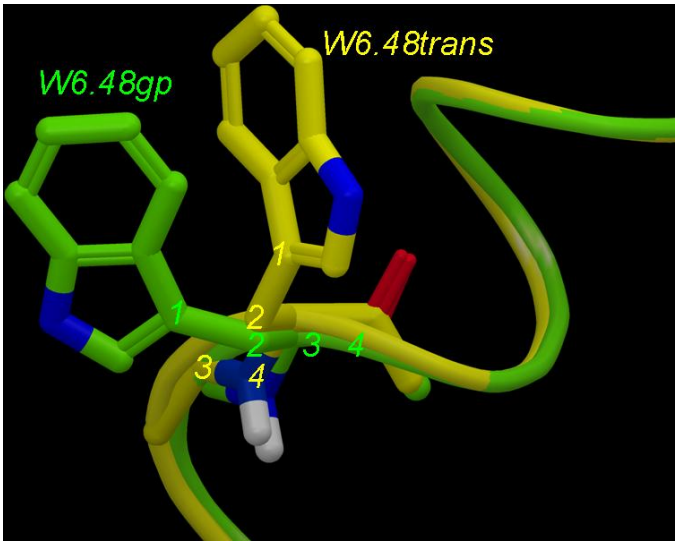

In Figure 4, the labels 1, 2, 3, and 4 represent the atoms that make up the dihedral angle. In *trans* (yellow 1, 2, 3, 4 atom labels) conformation the heavy atom 1 is opposite from the backbone N (atom number 4), while in *g plus* (green 1, 2, 3, 4 atom labels) conformation the heavy atom 1 is opposite from the backbone carbonyl carbon (atom number 4).

In the dark (inactive) state of Rho, the β-ionone ring of 11-cis-retinal is close to W6.48(265) of the TMH6 CWXP motif and helps constrain it in a χ_1 = *g*+ conformation (Palczewski, Kumasaka et al. 2000; Okada 2002; Li, Edwards et al. 2004). In the light activated

state, the retinal β -ionone ring moves away from TMH6 and toward TMH4 where it resides close to A4.58(169) (Borhan, Souto et al. 2000). The beginning of this movement is clear in the lumirhodopsin structure (Nakamichi and Okada 2006). This movement releases the constraint on W6.48(265), permitting this residue to undergo a conformational change. Both cryo-electron microscopy and NMR studies indicate that W6.48 changes position, as well as interaction partners during receptor activation (Schwartz and Rosenkilde 1996). This suggests that the conformation of W6.48(265) when Rho is in its inactive/ground state (R; χ_1 = *g*+) changes during activation (i.e., W6.48(265) χ_1 *g*+ to *trans*) (Shi, Liapakis et al. 2002). Toggle switch mechanisms for GPCR activation involving the W6.48 χ_1 *g*+ to *trans* transition have been proposed and tested for other GPCRs (Schwartz, Frimurer et al. 2006), including the β_1-AR (Shi, Liapakis et al. 2002) and the cannabinoid CB1 receptor (Singh, Hurst et al. 2002; McAllister, Hurst et al. 2004). Each of these mechanisms involves aromatic stacking interactions between W6.48 and other "toggle switch" residues (Yao, Parnot et al. 2006). With these reported findings in mind, the hypothesis in Specific Aim 1 was formulated and the Conformational Memories method was first tested using CB2 TMH6 as a case study for which experimental data is available for validation. In contrast to the more studied GPCRs, CB1 and CB2 have been shown to have a high level of ligand-independent activation, whereas rhodopsin is quite the opposite, as it exhibits an exquisite lack of constitutive activity. No data in this respect is available yet about GPR55. In this aim, it is hypothesized that a conformational change in χ_1 of W6.48 is also part of the activation process of CB2 receptor and that the lack of an aromatic residue at the position 6.44 may contribute to the increased constitutive activity of CB2 (relative to Rho) as was shown for CB1(Singh, Hurst et al. 2002). By looking at the sequence presented in Figure 5 it can be seen that Rho has aromatic residues at positions i-4 and i+3 from W6.48 (F6.44 and Y6.51,

respectively). A similar situation is present in the cationic neurotransmitter receptors, such as alpha-1B- and beta-2-adrenergic receptors, where W6.48 is flanked by F6.52 and F6.51 above and F6.44 below. In contrast to Rho and β_2-AR, in CB1 and CB2 these residues are Leu and/or Val (L/L6.44 and L/V6.51, respectively; Figure 5). In GPR55 these residues are F6.44 (i-4) and V6.51 (i+3). It has been reported that in the inactive state of Rho, F6.44(261) (χ_1 trans) interacts with W6.48 (265) (χ_1 g+). Han and coworkers reported that a F6.44 (261)V mutation in Rho led to measurable constitutive activity (Han, Smith et al. 1998). Chen and coworkers reported that a F6.44L mutation in the alpha-1B -adrenergic receptor and a F6.44L mutation in the β_2-AR receptor led to constitutively activated receptors, as well (Chen, Lin et al. 2001; Chen, Lin et al. 2002).

Figure 5. Alignment of the CB1, CB2, Rho, and GPR55 sequences in the TMH6 region.

Human Sequences

	6	6	6	6	6	6	6	6	6	6	6	6	6	6	6	6	6	6	6	6	6	6	6	6
	3	3	3	3	3	3	3	3	3	3	4	4	4	4	4	4	4	4	4	4	5	5	5	5
	0	1	2	3	4	5	6	7	8	9	0	1	2	3	4	5	6	7	8	9	0	1	2	3
	D	I	R	L	A	K	T	L	V	L	I	L	V	V	L	I	I	C	W	G	P	L	L	A
	D	V	R	L	A	K	T	L	G	L	V	L	A	V	L	L	I	C	W	F	P	V	L	A
	E	K	E	V	T	R	M	V	I	I	M	V	I	A	F	L	I	C	W	V	P	Y	A	S
	Q	K	A	C	I	Y	S	I	A	A	S	L	A	V	F	V	V	S	F	L	P	V	H	L
CB1	338	339	340	341	342	343	344	345	346	347	348	349	350	351	352	353	354	355	356	357	358	359	360	361
CB2	240	241	242	243	244	245	246	247	248	249	250	251	252	253	254	255	256	257	258	259	260	261	262	263
Rhodopsin	247	248	249	250	251	252	253	254	255	256	257	258	259	260	261	262	263	264	265	266	267	268	269	270
GPR55	221	222	223	224	225	226	227	228	229	230	231	232	233	234	235	236	237	238	239	240	241	242	243	244

In the above illustration of the alignment the last 5 residues of the helix are not shown. The Ballesteros-Weinstein numbers (Ballesteros and Weinstein 1995) and absolute sequence numbers for each are listed below the sequence comparison.

In Specific Aim 2, the refinement of the initial inactive state (R) of the GPR55 receptor model built in the Reggio's lab (Hurst, Barnett-Norris et al. 2006) was continued by exploring the

conformational space available to four flexible helices. The initial model was constructed from a template of the 2.65 Å crystal structure of bovine Rho (1GZM) (Li, Edwards et al. 2004) and with the aid of the MODELLER program (Fiser, Do et al. 2000; Marti-Renom, Stuart et al. 2000).

Figure 6. GPR55 topology.

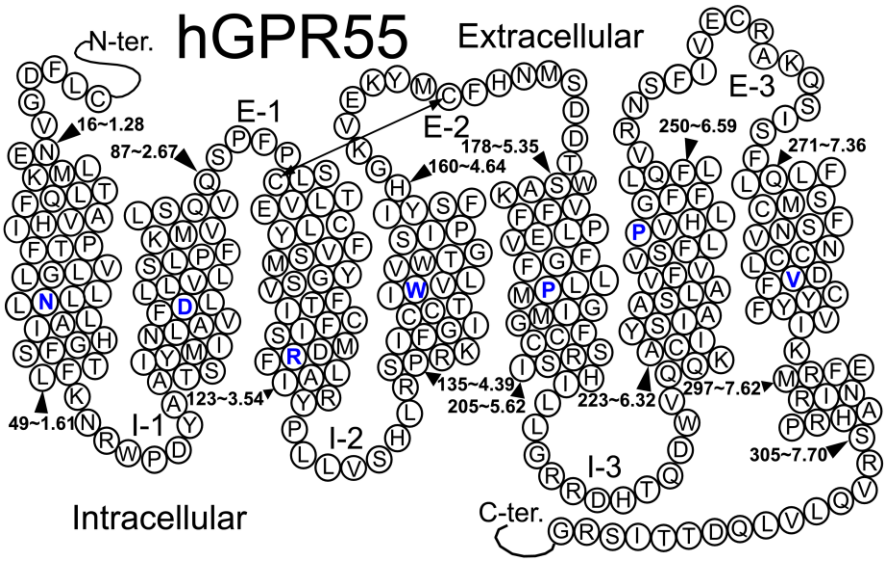

Figures 6 and 7 show representative views of the GPR55 model with some of the important features of its binding pocket. Dr Reggio's research group and collaborators have cloned and expressed the GPR55 receptor and preliminary studies confirm that multiple cannabinoid compounds activate this receptor.

Like CB1 and CB2, GPR55 has the following conserved residues among the Class A G-protein coupled receptors: N1.50, D2.50, W4.50 and P6.50. GPR55 also has P5.50 conserved, while CB1 and CB2 do not. The other conserved key motif of GPCRs found in GPR55 is the TMH3 DRY motif, with the conserved aromatic residue being F instead of Y in GPR55. Also,

the highly conserved TMH6 CWXP motif aligns with SFLP corresponding motif in the alignment of the TMH6 in GPR55 with other GPCRs. These residues parallel CWXP since S is a conservative substitution for C and since F is a conservative substitution for W. Another important similarity with Rho, but not to the classical cannabinoids, is the presence of F7.60 in the intracellular extension of TMH7, Hx8. The greatest divergence from Rho and the other cannabinoid receptors lies in the fact that the highly conserved NPXXY motif is replaced with DVFCY in GPR55.

Figure 7 illustrates key features of the preliminary GPR55 model built in the Reggio lab: charged residues in the binding site crevice of GPR55 are illustrated in yellow. In this model, the aromatic residues Y3.32, F3.33, Y3.37, H4.64, F5.39, F5.47, F6.48, H6.52, F6.55 and F6.59, shown in white, were identified as potential aromatic microdomains available for ligand interaction. Similar findings were reported to exist in CB1 (McAllister, Rizvi et al. 2003) and CB2 (Zhang, Hurst et al. 2005). In green, the residues that could H-bond are highlighted. Reggio has proposed that beta-branching residues (V6.43/I6.46) that face lipid on TMH6 may be a motif that helps pull endocannabinoids into the binding site of CB1 and CB2 (Barnett-Norris, Hurst et al. 2002) and recent mutation data supports this hypothesis (Reggio, Nebane et al. 2005). GPR55

Figure 7. GPR55 binding pocket.

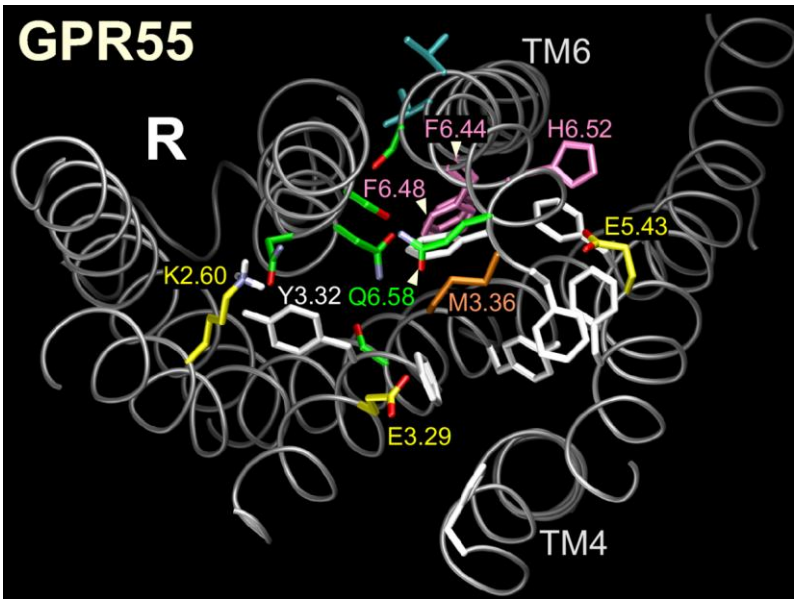

possesses on the lipid face of TMH6: V6.43/V6.46. These residues are displayed in blue in Figure 7.

2.3 Structure Creation and Minimization

Each helix of interest was built using Macromodel (Schrödinger Inc., Portland, OR, USA). The helix was first minimized using the AMBER* force field in Macromodel (Mohamadi, Richards et al. 1990). Each helix was then capped with acetamide at the N terminus and with N-methyl amide at the C terminus. The charges on all charged residues were reduced to one-third of their values to prevent artifacts during the CM runs. These artifacts occur because the runs were performed in vacuum and the individual helices studied were isolated from the naturally surrounding lipids and the rest of the receptor. When present, charged residues, which would

otherwise interact with surrounding native partners, in the system used, if left fully charged these residues would find each other and distort the structure of the helix.

2.4 Conformational Memories (CM) Method

The CM method (Guarnieri and Weinstein 1996) employs multiple Monte Carlo/ simulated annealing random walks and the united atom force fields AMBER* or CHARMM (PARAM19 force field). The runs were performed in vacuum and using a distance dependent dielectric. CM has been shown to converge in a very practical number of steps, and to be capable of overcoming energy barriers efficiently (Singh, Hurst et al. 2002). A new version of CM generated in the Reggio lab uses the CHARMM force field (Whitnell, Hurst et al. 2007). Force field methods have a long history (1946) and they rest on the fundamental concept of the ball and spring model and are used to approximate a molecule. Furthermore, it is assumed that the total energy of the molecule is a summation of the individual energy components such as bond stretching, angle bending, nonbonded interactions, torsion interactions, cross energy terms. The CM method has two phases: the exploratory phase and the biased phase.

2.4.1 Exploratory Phase

In the exploratory phase, a random walk is used to identify the region of conformational space that is populated for each torsion angle studied. Starting at a temperature of 2070 K or 3000 K, 50,000 steps are applied to the rotateable bonds with cooling in 18 steps to 310 K. Trial conformations are generated at each temperature by randomly picking 2 or 3 torsion angles from the set of torsion angles for each helix, and changing each angle by a random value within the range set in the calculation. After each step, the generated trial conformation is either accepted or rejected using the Metropolis criterion. Accepted conformations are used to map the

conformational space of each helix by creating 'memories' of values for each torsion angle that are accepted. The CM runs are performed in parallel, with either ten sets of 10 runs or four sets of 25 runs. Each set of runs uses a different random number seed. The output from these runs is combined to generate the 'memories' used for the biased annealing phase.

2.4.2 Biased Phase

In the second CM phase, only torsion angle moves that would keep the angle in the 'populated conformational space' mapped above are attempted. The Biased Annealing phase begins at a temperature of 722 K with cooling to 310 K in 8 steps. Runs are performed in parallel, with either ten sets of 10 or four sets of 25 runs, each using the combined 'memories' from the first phase of the calculation, but initiated with a different random number seed for the biased annealing phase of the calculation. Finally, 100 structures are output at 310 K. Conformational families of the flexible molecule/helix at 310 K are characterized from the results of the biased sampling technique by clustering conformations according to a pairwise root mean square deviation criterion (Mohamadi, Richards et al. 1990).

In the CM protocol used in this study, the phi (ϕ) and psi (ψ) angles of the region of the helix backbone thought to be the flexible hinge region were varied by ± 50°, while the rest of the helix backbone was only varied by ±10°. The chi (χ) angles were allowed to vary ±180° unless otherwise specified. Reggio's group has performed the control experiment in which all backbone ϕ and φ torsion angles were allowed to vary ±50°. In this experiment, they found that lower acceptance rates were obtained, but the same results for helix conformation were observed in the output structures, such that extreme variations from alpha helicity were seen only in regions containing helix distorting residues/motifs, such as the motifs containing prolines, serines, or

double glycines. This occurs because when CM tries a large ϕ and φ change in regions of the helix that do not contain helix distorting residues or motifs, the resultant high-energy helix conformations are not accepted by the Metropolis criterion.

2.5 Analysis

The proline kink (bend, B), wobble (W) and face shift (FS) angles for each set of 100 helices were calculated using the Prokink program (Mohamadi, Richards et al. 1990) available within the Simulaid package (M. Mezei, can be searched at the following web address: http://fulcrum.physbio.mssm.edu/~mezei/simulaid/). In this method the bend, wobble and face shift angles are as defined in Figure 7. The helix is described as being composed of two parts: the pre-proline helix (from the N-terminus to the proline residue) and the post-proline helix (from the C-terminus to the proline residue). The angle between the two parts is the bend angle. The wobble angle is defined as the angle between the projection of the post-proline helix to the yz plane and the C alpha atom of the proline and origin, as the C alpha is positioned on the positive y axis such that the center of the pre-proline helix is located on the positive x axis, as shown in Figure 7. The face shift angle is related to the bend and wobble angles and measures the twist that occurs in the helix due to the proline kink. If one looks from a side, in an ideal alpha helix the amino acids i-4 and i-3 from the proline, are located on the same side of the helix. In a bent helix, these residues are shifted in a bent helix, such that they are on different sides (see Figure 8).

In Specific Aim 1, the criterion that W6.48 undergoes a shift in its χ_1 (g+ to trans) during activation was used (Lin and Sakmar 1996). The W6.48 χ rotamer states of the resultant helices were assessed according to the number of helices of each TMH6 (WT CB2 for wild type CB2, L6.44F mutant CB2), which exist in an inactive (W6.48 g+ χ_1) vs. an active (W6.48 trans χ_1)

W6.48 χ_1 rotamer state. The Prokink program was applied around P6.50 of TMH6 in CB2 with the flexible region varied from I6.46 to P6.50 (ICWFP). In Specific Aim 2, the Prokink Analysis was performed similarly on the last residue of the flexible region varied: for TMH2, the flexible region was from V2.54 to P2.58 (VLSLP), for TMH5 flexible regions (one at a time) were: K5.37 to P5.41 (KVFFP), G5.46 to P5.50 (GFLLP), M5.51 to G5.55 (MGIMG), for TMH6 the flexible region was V6.46 to P6.50 (VSFLP), and for TMH7 the flexible region was C7.46 to V7.50 (CCLDV).

Figure 8. Illustration of the structural parameters of the proline bend angle, wobble angle and face shift.

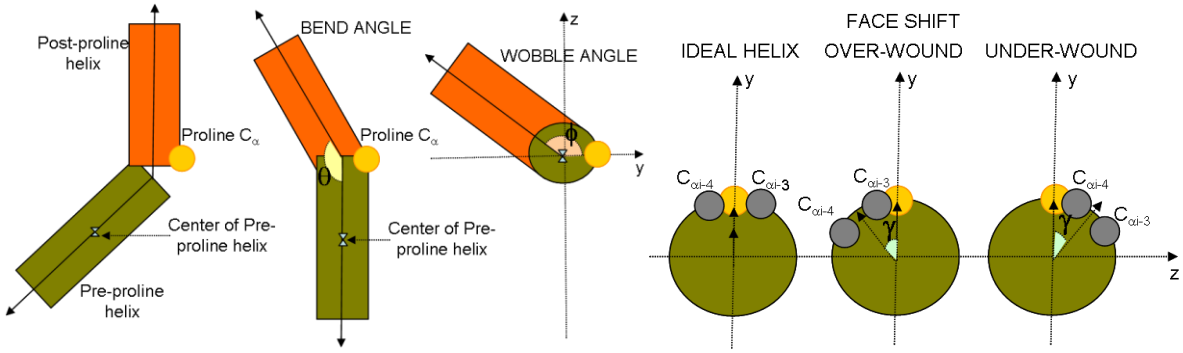

For the exploration of the influence that bracketing aromatics have upon 6.48 conformation in the cannabinoid receptors, the previously developed protocol for TMH6 studies was used (Singh, Hurst et al. 2002). We looked for the pattern of aromatic residue χ_1 torsion angles when the χ_1 of 6.48 is in g+ (inactive state conformation) vs. when the χ_1 of 6.48 is in trans (active state conformation) (see section 1.4.2 Activation of GPCRs) to see if there are correlations between the aromatic χ_1 torsion angles that would suggest a uniform movement of these residues as 6.48 moves from a g+ χ_1 to a trans χ_1. Such a correlation would suggest that

these flanking aromatics act as a “toggle switch” or may explain the degree of constitutive activity.

2.6 Experimental Procedures (Collaborator)

The following experimental procedures are only briefly described and referenced to the work done in Dr Zhao-Hui Song’s lab at University of Louisville School of Medicine.

2.6.1 Ligand Binding Assay

Ligand binding assays were performed as described previously (Zhang, Hurst et al. 2005) with slight modifications. For membrane preparations, cells were washed twice with cold PBS (8.1mM NaH2PO4, 1.5mM KH2PO4, 138mM NaCl, 2.7mM KCl, pH 7.2) and scraped off the tissue culture plates. Subsequently, the cells were homogenized in binding buffer (50 mM Tris–HCl, 5 mM MgCl2, 2.5 mM EDTA, pH 7.4) with a Polytron homogenizer. After the homogenate was centrifuged at 34,000 g for 30 min at 4°C, the pellet was resuspended in binding buffer and 10 stored at -80°C until use. Protein concentrations were determined with Bradford method using Bio-Rad protein assay reagent (Bio-Rad, CA). Bovine serum albumin (BSA) was used as the standard. For binding assays, cannabinoid ligand dilutions were made in binding buffer containing 0.5 mg/ml of BSA and then added to the assay tubes. [3H]-CP55940 was used as a labeled ligand for competition binding assays. Nonspecific binding was determined in the presence of 1⌈M unlabeled CP55940. Binding assays were performed in 0.5 ml of binding buffer containing 0.5 mg/ml of BSA for 60 min at 30°C. Free and bound radioligands were separated by rapid filtration through polyethylenimine-treated GF/B filters (Whatman International) with a Brandel cell harvester (Gaithersburg, MD). The filters were washed three times with 3 ml of cold

wash buffer (50 mM Tris–HCl, pH 7.4, containing 1 mg/ml of BSA). The bound [3H]-CP55940 was determined by liquid scintillation counting after overnight equilibration in 5 ml of scintillation fluid (MP Biomedicals, Irvine, CA). The assays were performed in duplicate, and the results represent the combined data from at least three independent experiments.

2.6.2 Assay of cAMP Accumulation

cAMP accumulation assays were performed using a method described previously by (Song and Bonner 1996). Briefly, cells were grown to confluence, washed twice in PBS containing 0.5 mM EDTA, and then collected in DMEM containing 0.2% (w/v) fatty acid free BSA. Subsequently, the cells were centrifuged at 500×g for 5 min at 25°C, and resuspended in 10 ml of DMEM containing 0.2% (w/v) fatty acid free BSA. After counting the cell number, the cell suspension was diluted to 2×106 cells per milliliter. To prevent the hydrolysis of cAMP, the cells were incubated with 0.2 mM RO20-1724, a phosphodiesterase inhibitor, for 10 min before stimulation. The stimulation was initiated by adding aliquots of cells to silanized test tubes containing forskolin with or without cannabinoids and incubated for 10 min at 37°C. The final 11 assay volume was 250µl with 4×105 cells per tube. For ligand-induced inhibition of cAMP accumulation assays, we used a final forskolin concentration of 1µM and a series of concentrations of CP55940. For constitutive activity assays, cells were stimulated by different concentrations of forskolin (0.1-10µM) with or without 1 µM CB2 specific inverse agonist SR144528. The reaction was stopped with the addition of 250µl of stop solution (0.1 M HCl, 0.1mM CaCl2), after which 50µl was removed for cAMP radioimmunoassay, using a kit from PerkinElmer (Boston, MA).

CHAPTER III

RESULTS AND DISCUSSION

3.1 Specific Aim 1 – Computational Method Optimization

3.1.1 Computational Results

The force field employed (AMBER* or CHARMM) and the helix starting structure were compared while exploring the conformational mobility of the peptide. The method used was the biased Monte Carlo/simulated annealing Conformational Memories (CM), which is described in the Research and Design Methods Section. TMH6 is important in the activation of CB2, as well as in other GPCR's. For this reason, the conformations that are possible could give insight in the ligand-receptor and ligand-independent activation of the receptor. Relevant experimental data is also available for validation from Zhao-Hui Song's lab (R. Zhang et al., manuscript submitted 2010), which is presented in the Experimental Results section (see Table 2).

Two different starting conformations were used. In **Starting Conformation I**, the human WT CB2 TMH6 and an L6.44F mutant were built using Macromodel (Schrödinger Inc., Portland, OR, USA) and minimized using the AMBER* force field in Macromodel (Mohamadi, Richards et al. 1990). In **Starting Conformation II**, TMH6 from the rhodopsin crystal structure (1GZM) was mutated to the corresponding CB2 residues using Maestro and the side chains (but not the helix backbone atoms) were minimized using the AMBER* force field in Macromodel (Mohamadi, Richards et al. 1990).

In this aim, it was hypothesized that a change in the conformation of W6.48 is part of the activation process of CB2 receptor and that the lack of an aromatic residue at the position 6.44

could increase constitutive activity of this receptor like it was shown for CB1(Singh, Hurst et al. 2002). By looking at the sequence presented in Figure 4 (Introduction Section), the Rho sequence has aromatic residues at positions i-4 and i+3 from W6.48 (F6.44 and Y6.51, respectively). A similar situation is present in the cationic neurotransmitter receptors, such as the α-1B- and beta-2-adrenergic receptors, where W6.48 is flanked by F6.52 and F6.51 above and F6.44 below. Unlike Rho and β_2-AR, the cannabinoid receptors have Leu and/or Val (L/L6.44 and L/V6.51, respectively; Figure 3). It has been reported that in the inactive state of Rho, F6.44(261) (χ_1 trans) interacts with W6.48 (265) (χ_1 g+), while Han and coworkers reported that a F6.44(261)V mutation in Rho led to measurable constitutive activity (Han, Smith et al. 1998). Similarly, Chen and coworkers reported that a F6.44L mutation in the α-1B-AR and a F6.44L mutation in the β_2-AR receptor led to constitutively activated receptors, as well (Chen, Lin et al. 2001; Chen, Lin et al. 2002). For this reason the L6.44F mutant was studied here with the F6.44 χ_1 constrained in either a *g plus* or *trans* conformation (see Table 1).

In Table 1, the results of the rotamer distribution for the W6.48 χ_1 for the WT runs show that in Starting Conformation I there is a preference for the W6.48 χ_1= *g plus* (inactive), while in the Starting Conformation II the populations of *g plus* or *trans* are equal. In the case of the L6.44F mutant runs, regardless of the starting conformation of the original TMH6, Conformational Memories calculations suggest that over 95% of the population of the output helices have W6.48 in the inactive state conformation (χ_1= *g plus*) when F6.44 adopted a conformation of χ_1 = *g plus*. The *trans* population for W6.48 $\chi_1$is preferred in over 60% of the helices when F6.44 has a conformation of χ_1 = *trans*.

Table 1. Summary of CB2 WT and L6.44F mutant runs: Percentage Rotamer Populations (χ_1) of W6.48 and corresponding Prokink Data.

CB2 TMH6	**Constrained Residue (F6.44 in mutants)**	**W6.48 χ_1 conformation in the output structures**		**Bend (B)**		**Wobble (W)**	**Face Shift (FS)**
Starting Structure I or II	χ_1	# of Structures	χ_1	average	range	average	average
WT-I	N/A	13	*t*[a]	23.93	[18.3 – 32.5]	140.62	-18.95
		87	*g* +[b]	20.70	[12.9 – 32.6]	123.84	-18.39
L6.44F-I	100 *g*+	3	*t*	22.92	[17.9 -28.6]	116.44	-35.05
		97	*g* +	22.07	[12.6 – 37.2]	127.55	-20.35
L6.44F-I	100 *trans*	63	*t*	21.63	[11.8 – 37.6]	118.44	-20.13
		37	*g* +	19.57	[11.5 – 26.5]	120.68	-26.05
WT-II	N/A	48	*t*	28.37	[11.0 – 47.5]	-72.70	95.46
		52	*g* +	25.90	[5.3 -43.7]	-80.41	94.06
L6.44F-II	100 *g*+	4	*t*	25.88	[7.0 – 35.9]	-63.20	92.86
		96	*g* +	27.56	[9.8 – 47.2]	-78.60	93.49
L6.44F-II	100 *trans*	66	*t*	28.34	[13.8 - 48.8]	-81.75	95.87
		34	*g* +	27.33	[11.2 – 47.5]	-73.12	96.83

[a] *trans* and [b] *g plus*

The results of Prokink Analysis for WT CB2 TMH6 **Starting Conformation I** are also presented in Table 1. The first three entries in the table represent the WT and L6.44F runs of the TMH6 helix built in **Starting Conformation I**, while the last three entries represent the WT and

L6.44F runs of the TMH6 helix built in **Starting Conformation II**. The force field used in these calculations was AMBER*. The bend angle (B) is the angle between the two parts of the helix that are on each side of the proline residue. For the TMH6 structures in which the W6.48 χ_1 is *trans* this angle was found to be slightly larger than for the helices in which the W6.48 χ_1 is *g plus* (Table 1, and Figures 8, 9 and 10), however, because the ranges overlap between the two populations, this trend is not statistically significant. This trend in bend angle is the opposite of that seen in CB1(Singh, Hurst et al. 2002). The bend appears biased by the starting conformation, such that whether wild type or mutant, the helices from Starting Structure II with W6.48 in *g+* or in *trans*, show a slight trend towards being more bent than the corresponding helices from the Starting Structure I runs.

Figure 9 illustrates bend and wobble angle ranges for CB2 receptor wild type. Helices from the Starting Structure II are more bent than those from Starting Structure I. Helices that have W6.48 $\chi_{1 =}$ *trans* are slightly more bent on average than those with $\chi_{1 =}$ *g+*. Helices from Starting Structure I have positive wobble angles and negative face shift angles (over-wound), while helices from Starting Structure II (darker colors) have negative wobble angles and positive face shift angles (under-wound). In Figure 9A Starting Structure I is represented in light colors (light green for the W6.48 $\chi_{1 =}$ *g+* helices and yellow for the W6.48 $\chi_{1 =}$ *trans* helices). In Figure 9B Starting Structure II is illustrated in dark colors (dark green for the W6.48 $\chi_{1 =}$ *g+* helices and orange for the W6.48 $\chi_{1 =}$ *trans* helices). In Figure 9C Starting Structure I and II are overlaid. The output helices are superimposed intracellularly (first 10 residues). The views are from the extracellular side (bottom of each figure) and from the transmembrane side (right of each figure).

Figure 9. Bend and wobble angle ranges for the wild type CB2 receptor.

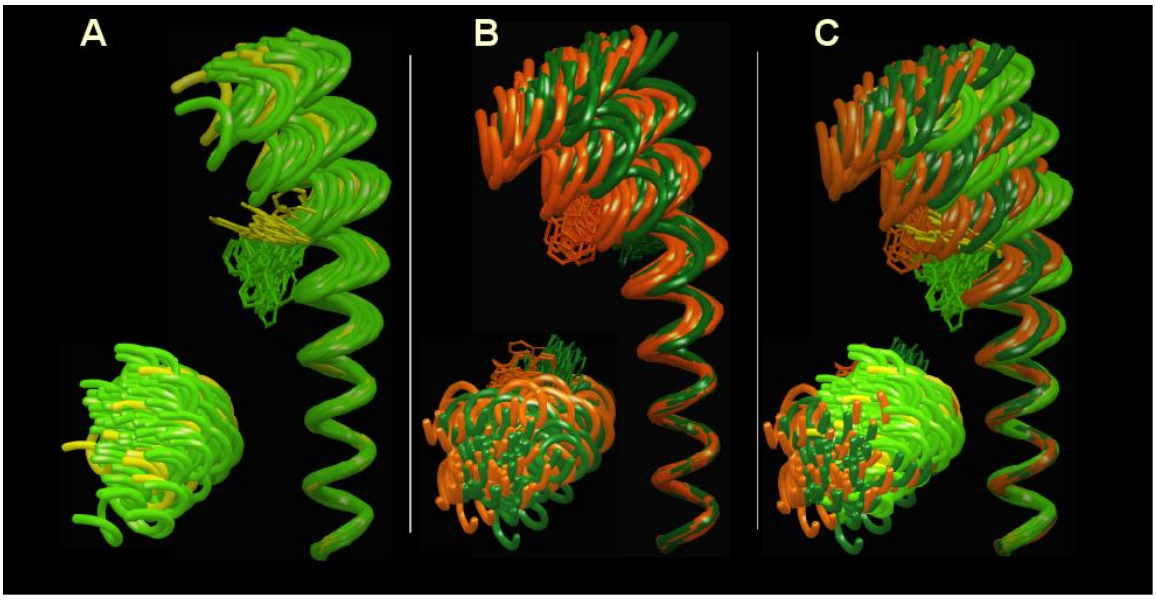

As mentioned in the Methods section, the wobble angle (W) is the angle that describes the orientation of the post-proline helix (the part from the proline residue to the C-terminus) with respect to the pre-proline helix (the part from the proline residue to the N-terminus) in 3D. From Table 1 it can be seen that the wobble angle of the output helices from Starting Conformation I is significantly different from the Starting Conformation II in both wild type and mutant helices (Figures 9 and 10).

Figure 10 shows a comparison between Starting Structure I and II wobble angle ranges for wild type (WT) and mutant (MT) output helices. The helices are shown as they are superimposed on the extracellular backbone composed of the last 10 residues (post proline). Both intracellular and side views are illustrated. In the left side of the figure (**A**) the helices in which W6.48 conformation was *g+* are shown, while on the right hand side of the figure (**B**) the W6.48 *trans* helices are shown. Figure 10 shows that the wobble angles are significantly different

depending on what starting structure is used: I versus II, while the wobble angles are not significantly different between helices within the same starting structure.

Figure 10. Comparison between Starting Structure I and II wobble angle ranges for wild type (WT) and mutant (MT) output helices.

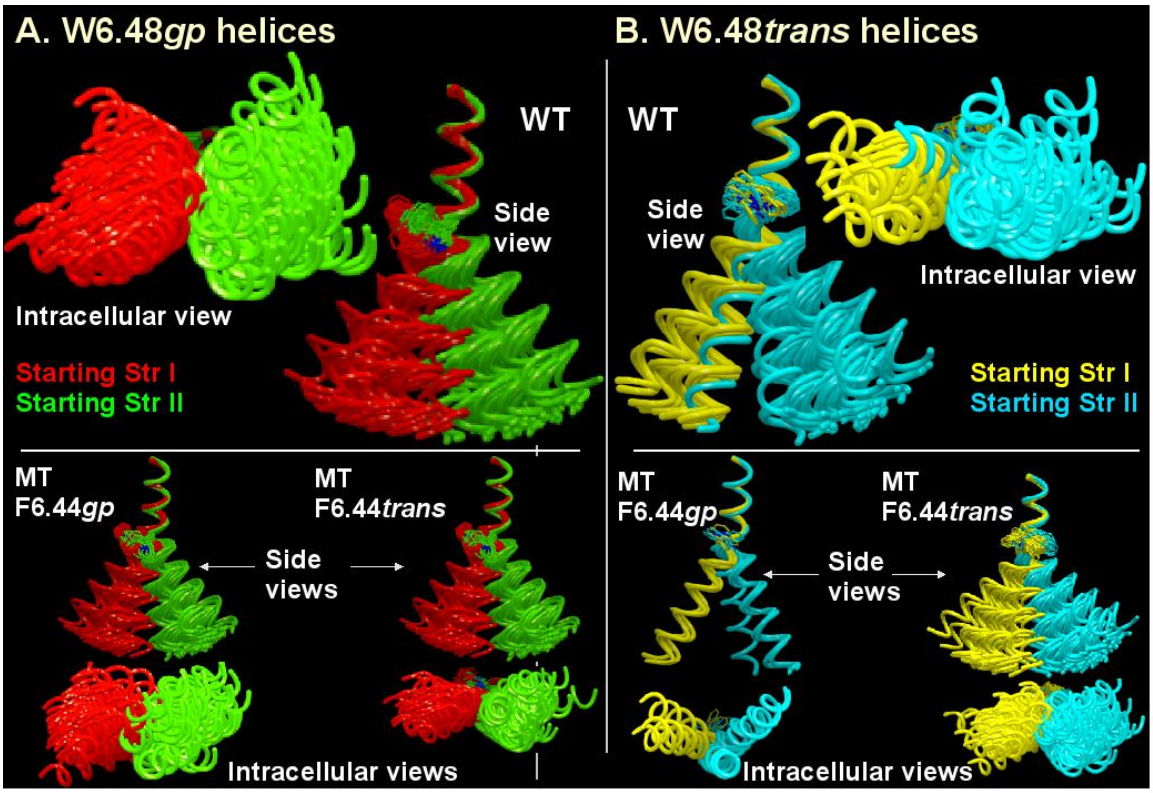

The face shift angle is related to the bend and wobble angles, hence it is also very different between the two starting conformations, but it still represents a useful indicator because it measures the distortion that causes a twist in the helix such that residues that were on the same side of the helix will be on different sides because of the bend caused by the proline. The atoms involved in this distortion are i-4 and i-3 from the proline (see Figure 8 in Methods Section). A negative shift, as is observed in the output helices from the Starting Structure I, imply that the

helix is over-wound as a result of the proline kink. In contrast, the helices from Starting Structure II are under-wound.

Figure 11. Comparison between Starting Structure I and II wobble angle ranges for wild type (WT) and mutant (MT) output helices.

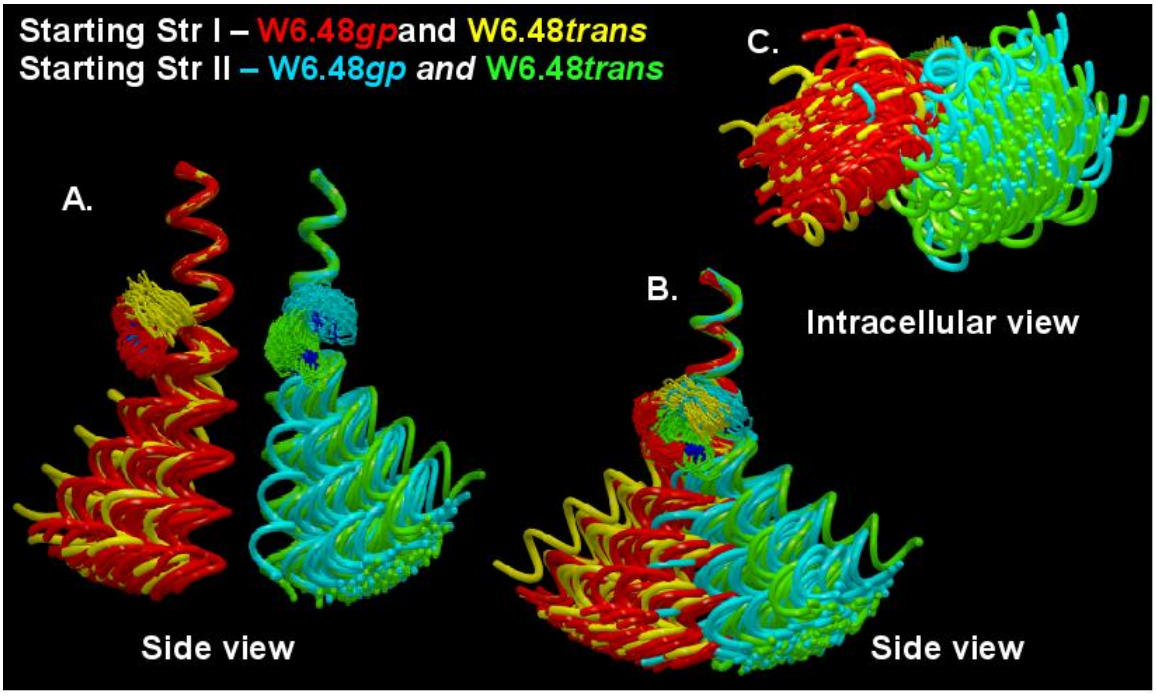

To the left in Figure 11 A, there is an illustration of output helices from all the runs from Starting Structure I (WT, MT with F6.44 constrained *gplu*s and *trans*) superimposed on the extracellular last 10 residues and colored in red and yellow depending on the W6.48 conformation and the output helices from all the runs from starting structure II superimposed on the extracellular backbone composed of the last 10 residues (represented in blue and green according to the W6.48 orientation. In the center of the figure 11 B., all of the output helices from Starting Structure I and II are superimposed on the extracellular end showing that the two populations from Starting Structure I wobble in opposite direction from Starting Structure II. In

part C. of the figure 11 the same helices as in B are shown when viewed from the intracellular side.

Figure 12. Wild type CB2 TMH6 results from Starting Structure I and II runs.

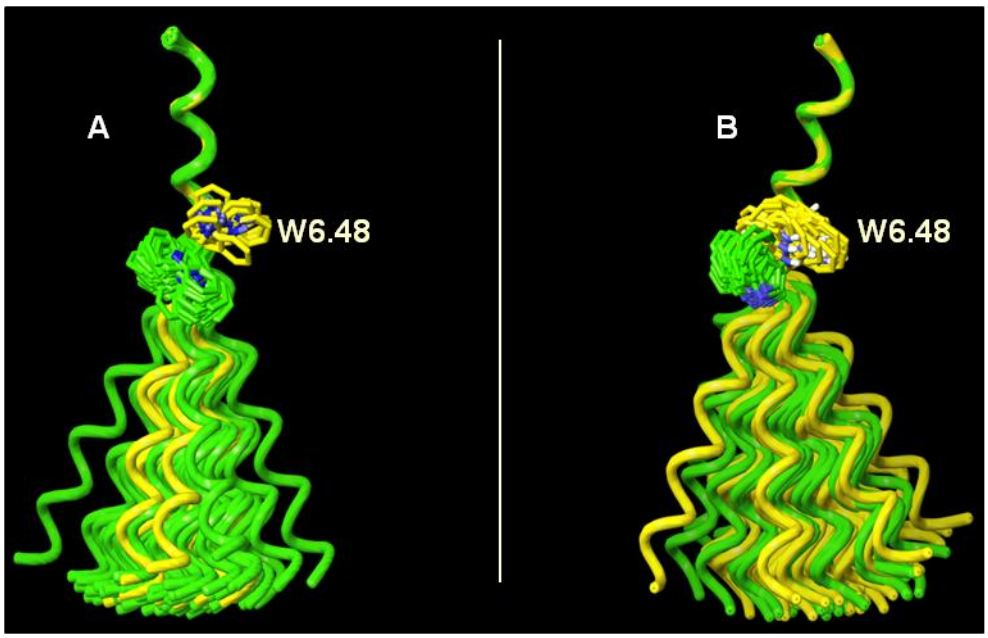

In Figure 12 A and B show the results of the WT CB2 TMH6 runs in Starting Conformation I and II, using AMBER* force field. The output helices for each run are superimposed on their extracellular ends starting with the backbone atoms of the Proline residue and moving up towards the end of the helix. Starting Structure II resulted in a higher population of W6.48 χ_1 = *trans* (see Table 1).

Figure 13. L6.44F CB2 TMH6 mutant results from Starting Structure I runs.

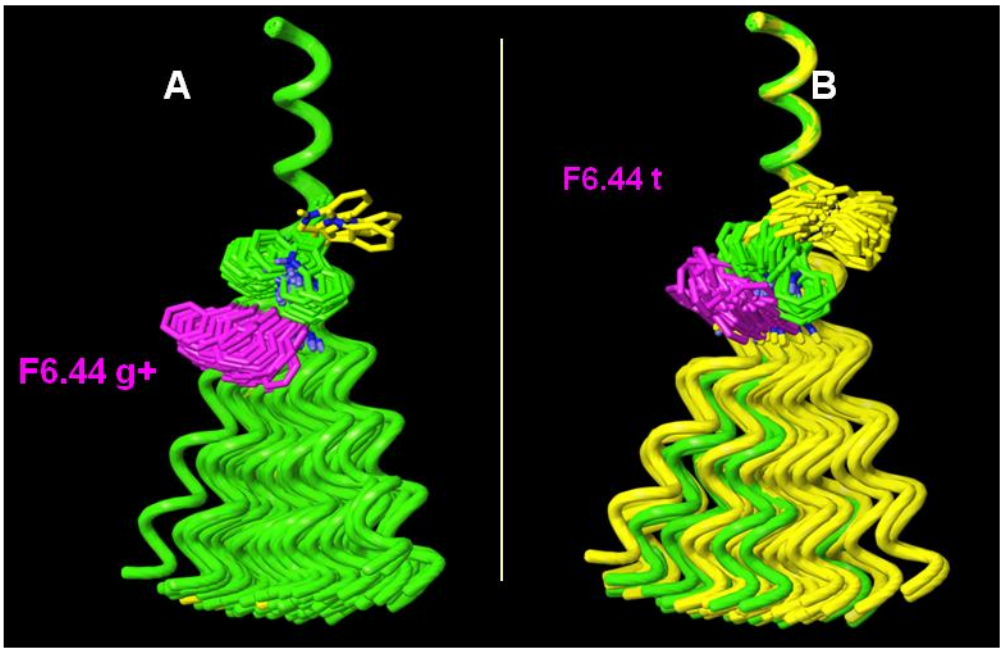

In the above Figure 13 A and B the results shown include only the Starting Structure I runs since the same findings were obtained when Starting Structure II was used.

Again the force field employed was AMBER*. The output helices for each run are superimposed on their extracellular ends starting with the backbone atoms of the Proline residue and moving up towards the end of the helix. The figure illustrates that when F6.44 is in a *trans* χ_1 conformation, it favors a W6.48 *trans* χ_1, while when F6.44 is in a *g*+ χ_1, it overwhelmingly favors a W6.48 *g*+ χ_1.

When the human WT CB2 TMH6 was run in a similar way but using the CHARMM force field instead of the AMBER*, the percent of χ_1 of W6.48 in *trans* (active state) was 20%, which is consistent with the Conformational Memories run on the same helix using the Amber * force field. However, due to other unpublished results of experiments done in Reggio's lab in

which CHARMM force field runs gave better results, this was the force field chosen for the CM runs in Specific Aim 2 for GPR55 helices.

In conclusion, the bend, wobble and face shift showed dependency on the starting conformation of the helix in a consistent manner. The Starting Structure II helices were more bent than the ones obtained from the Starting Structure I and they were over-wound as a result of this bend, while the ones from the Starting Structure I were under-wound (negative face shift values), such that the helices from the rhodopsin template (II) twist away from the W6.48, while the ones build from Macromodel twist over the tryptophan. However, regardless of the starting structure, the bend was slightly higher in the helices with W6.48 in the *trans* configuration. The wobble and face shift varied only slightly within a Starting Structure set, according to the W6.48 χ_1 angle or according to wild type vs. mutated helices. The W6.48 population was different between Starting Structure I with it being predominantly *g+*, while Starting Structure II generated similar percentages of *g+* and *trans*.

3.1.2 Experimental Results (Collaborator)

The following experimental results were obtained in Dr Zhao-Hui Song's lab at University of Louisville School of Medicine.

Table 2. Competition of specific [^{3}H]-CP-55940 binding to wild type and mutant CB2 receptor by CP55940 and SR144528. CI: Confidence Interval

Type	**CP55940**		**SR144528**	
	Kd (95%Cl), nM	**n**	**Ki(95%Cl), nM**	**n**
CB2 wild type	0.79(0.39-1.62)	10	14.8(9.49-23.3)	7
CB2 L644F mutant	4.47(1.38-14.5)	6	55.0(52.0-58.2)	3

Adenylyl cyclase is an enzyme that catalyzes the conversion of ATP to cAMP. CB2 receptors couple to Gi/o proteins that inhibit the enzyme adenylyl cyclase, thus decreasing the levels of cAMP. In this study, forskolin, which is able to activate adenylate cyclase by itself, was used in order to raise the levels of cAMP and resensitizing the cell receptors. Because CB2 receptors are constitutively active (CA), they reduce the cAMP levels in the absence of agonists. If an antagonist is added, such as SR144528, the activity of the cannabinoid receptor is reduced and therefore its effects on adenylyl cyclase are diminished and the levels of cAMP increase. If the receptor is not present though, the addition of the antagonist has no effect on the levels of cAMP. This is observed in Figure 14 A in which CB2 receptor was present and the levels of cAMP increase when the antagonist was added, thus preventing the cannabinoid receptor from inhibiting adenylyl cyclase. In contrast, in Figure 14B in which there is no CB2 present, the addition of the antagonist has no effect on the cAMP levels. Once the existence of the receptor was verified, Figure 15 shows that the L6.44F mutant has lost its constitutive activity and the addition of antagonist had no effect on the levels of cAMP.

In Figure 14 A CB2 inverse agonist (1mM), SR144528, prevented wild type CB2 receptor from decreasing cAMP level. In contrast, SR144528 had no such effect in untransfected HEK293 cells.

Figure 14. Constitutive activity of the wild type CB2 receptor.

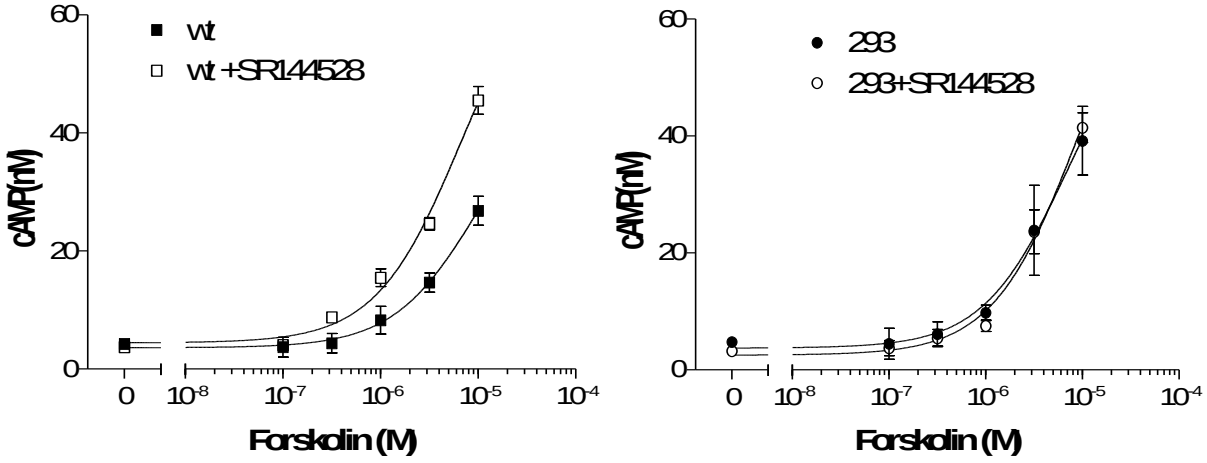

Experimental results for CB2 L6.44F show that while CP55940 has similar affinity for WT CB2 vs. the L6.44F mutant (see Table 2), the affinity of SR144528 at L6.44F is diminished 3.7 fold relative to WT. This decrease in affinity is unexpected since the L6.44F mutant shows reduced CA (constitutive activity), indicating the receptor population is in the "off" state, the state for which SR has higher affinity. It may be that the L6.44F mutation has had an effect on the SR144528 binding pocket and consequently, this results in reduced SR affinity.

Figure 14A shows that WT CB2 is a constitutively active (CA) receptor. Consequently, a preference for the W6.48 χ_1 = *trans* state would be expected for the WT receptor. CM calculations of WT CB2 TMH6 (Starting Structure II) revealed a preference for the W6.48 χ_1 = *trans* (activated) state conformation, while calculations with (Starting Structure I) did not. Taken together these results suggest that CM runs should employ an initial Rho template for the Starting Conformation of the helices.

Figure 15. SR144528 did not affect the basal level of cAMP in the L6.44F mutant, indicating reduced constitutive activity for this mutant.

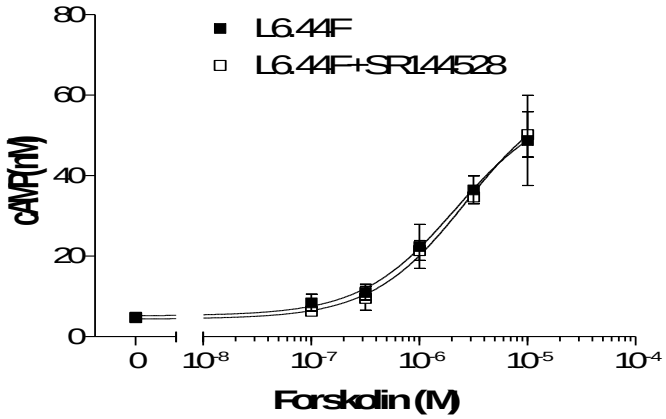

Figures 15 shows that the L6.44F mutant (Figure 15) has greatly diminished constitutive activity compared to WT (see Figure 13, left). These results are consistent with the modeling results presented here, which suggest that the χ_1 of residue 6.44 influences the χ_1 of W6.48 (see Table 1). Since in the context of the full CB2 bundle, an F at 6.44 can only exist in a $\chi_1 = g+$ (Hurst, Grossfield et al. 2010), the modeling studies suggest that W6.48 will remain in the $\chi_1 = g+$ (inactive state). This, in turn, should result in diminished constitutive activity in the mutant.

3.2 Specific Aim 2: Refinement of R State Model of GPR55

The GPR55 model was first refined based on computational refinements of the models. The initial model of GPR55 reported here in the Introduction section (Figure 6) is based upon a rhodopsin (Rho) template (1GZM structure). As mentioned previously, from Reggio's work with CB1/CB2, although the rhodopsin crystal structure is a good starting point for the cannabinoid receptor modeling, there are sequence dictated differences between rhodopsin and each of these receptors. These differences can be manifested by the absence of a key motif, by divergent locations of proline or glycine residues, as well as by the presence of serines or threonines at key

positions, which can have important effects upon helix conformations. The biased Monte Carlo/simulated annealing Conformational Memories method, which was selected in Specific Aim 1 and described in the Research and Design Methods section, was used to study such sequence dictated divergences in key helices from the Rho template in GPR55. This technique has been successfully used previously to identify important differences from Rho in TMH6 of CB1 and CB2 (Barnett-Norris, Hurst et al. 2002) and to demonstrate a divergence in the TMH2 structure of CB2 from that of Rho (Zhang, Hurst et al. 2005).

Conformational Memories (CM) calculations for the GPR55 transmembrane helices were performed using a rhodopsin template starting conformation of the helices and the CHARMM force field. (**1) TMH2.** The first helix studied was TMH2, which in Rho does not have a proline, but does have a helix distortion from G2.56 to T2.59 (GGFT). The GGFT sequence is not found in GPR55, but the proline at 2.58 could mimic the structural distortion of the GGFT. Therefore the flexible region was considered to be from V2.54 to P2.58 (GPR55). **(2) TMH5**. The next important helix to study was TMH5. In Rho, there is a single proline residue in TMH5 at position 5.50, which causes a deviation from normal alpha-helicity in the region, 5.46-5.50. TMH5 in GPR55, however, has two proline residues (P5.40 and P5.50) and three glycine residues (G5.46, G5.52 and G5.55), which also could cause distortions from normal alpha-helicity. For this reason the possibility of three regions of flexibility in this helix were considered: K5.37- P5.41 (KVFFP), G5.46-P5.50 (GFLLP), and M5.51-G5.55 (MGIMG). (**3) TMH6.** The next helix considered was TMH6, which in GPR55 does not have the highly conserved CWXP motif, so typical of the Class A GPCR, but has the conservative substitutions of this motif: SFLP in GPR55. Because this helix has been implicated in conformational changes during receptor activation, it was important to study the allowed conformations of this helix by considering the

region from V6.46 to P6.50 as the flexible part. **(4) TMH7.** Lastly, the TMH7 helix was studied considering the C7.46 to V7.50 (CCLDV) region as the flexible region.

The CM results for TMH2, 5, 6 and 7 are presented in Table 3 and Figures 16-19 below.

Table 3. Summary of the Average Bend, Wobble, and Face Shift angle results for GPR55 TMH2, TMH5, and TMH6 runs.

GPR55	**Average Bend (B)**	**Average Wobble (W)**	**Average Face Shift (FS)**
TMH2 (V2.54-P2.58)	25.72	-112.97	25.30
TMH5 (K5.37-P5.41)	8.23	82.80	9.02
TMH5 (G5.46-P5.50)	11.97	-113.36	66.42
TMH5 (M5.51-G5.55)	7.86	1.53	14.16
TMH6 (V6.46-P6.50)	24.85	-105.24	51.93

The TMH7 output structures obtained were highly bent and not suited to be used in the receptor model; therefore the statistical data for TMH7 is not included in the table above (see Figure 16).

Figure 16. CM results for TMH7 of GPR55.

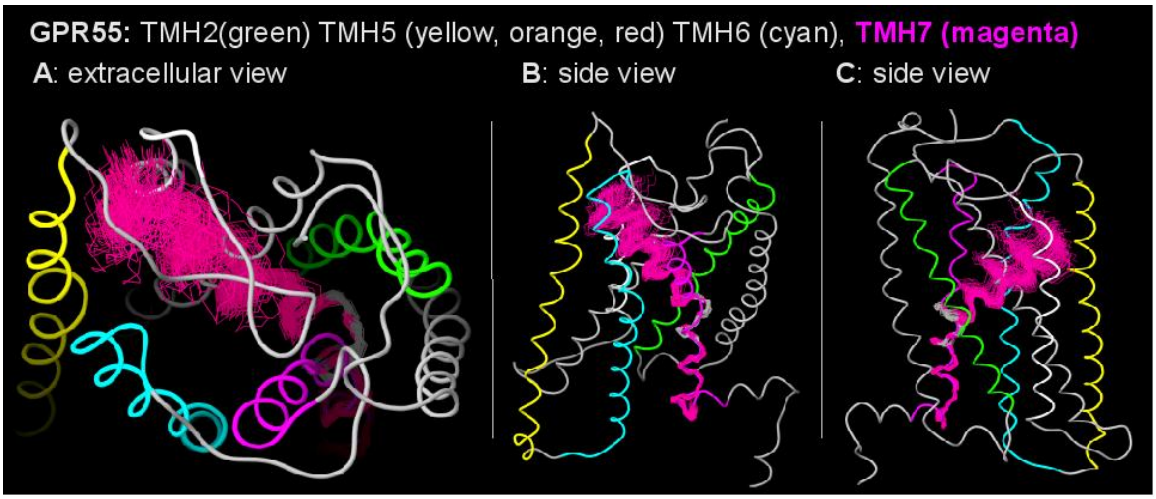

Figure 17. CM results for TMH2, TMH5, and TMH6 of GPR55.

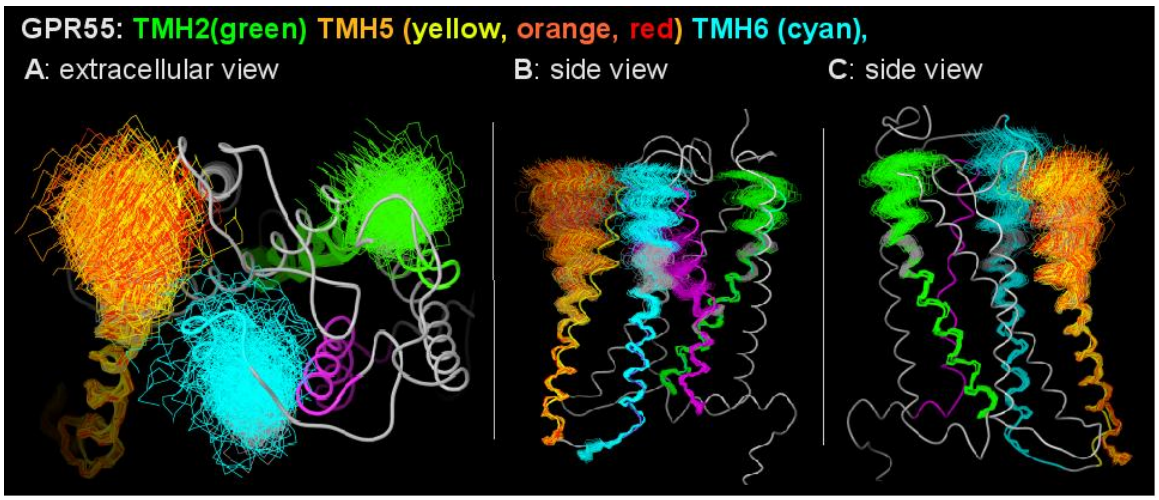

In Figure 17, the output structures for each helix run are superimposed intracellularly and placed in the context of our GPR55 model described in the Introduction section (see Figure 6).

Figure 18. CM results for TMH2, TMH5, TMH6 and TMH7 of GPR55

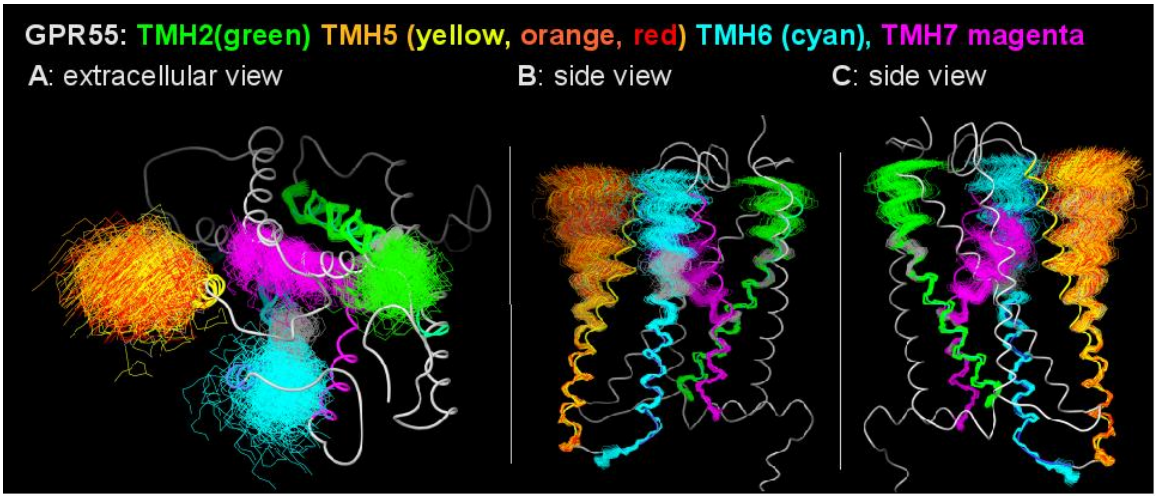

Figure 18 illustrates the extracellular view of the conformational memories results for TMH2 (green), TMH5 (red/orange/yellow), TMH6 (cyan) and TMH7 (magenta) of GPR55 (A) and side views in B and C. As in Figure 17, the output structures for each helix run are superimposed intracellularly and placed in the context of our GPR55 model described in the Introduction section (see Figure 6).

TMH2

From Figures 16 -17 above, it can be seen that the TMH2 population wobbles toward TMH3 when compared to the rhodopsin template. Extracellular loop EC1 between TMH3 and TMH2 is 3 residues shorter in GPR55 than in Rhodopsin, so TMH2 helices that reach over towards TMH3 would be preferred for use in a GPR55 model.

Figure 19. CM results for each of the region varied in TMH5.

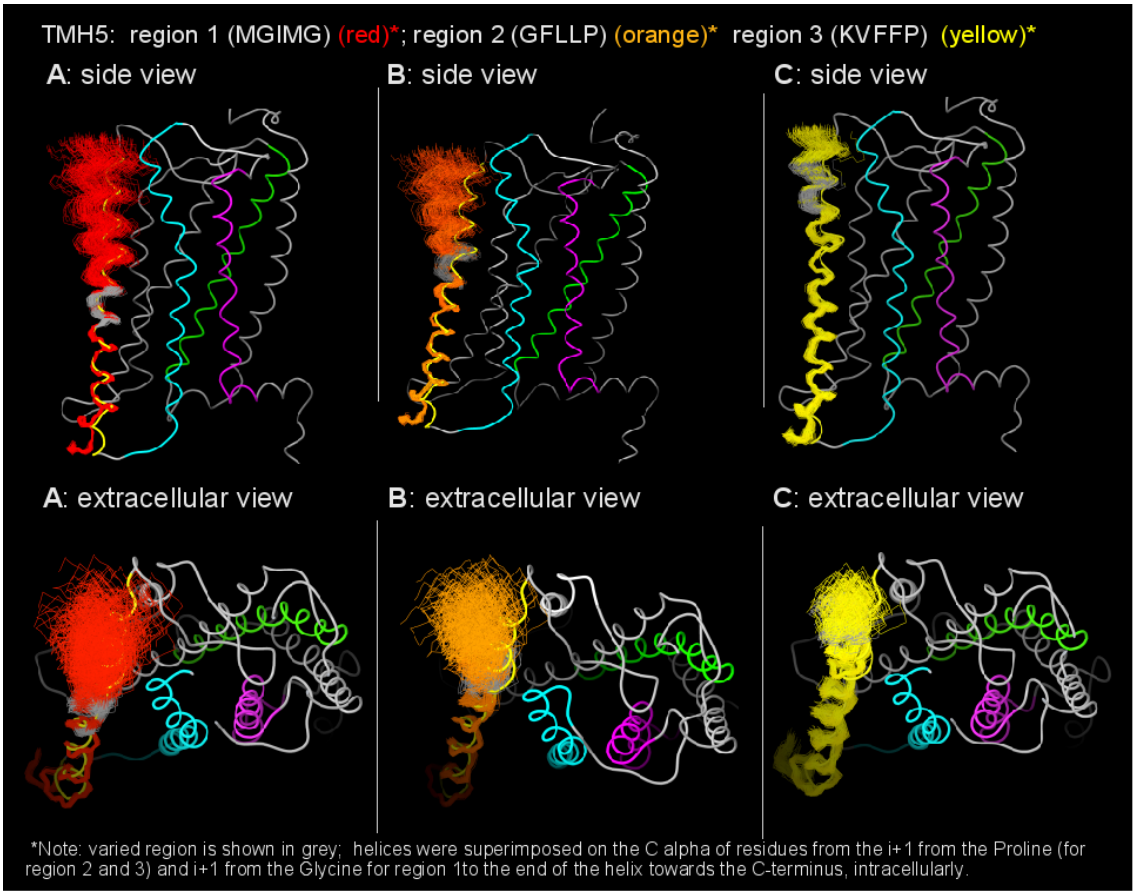

TMH5

Similarly, from Figures 16-18, it can be seen that TMH5 population bends away from the template transmembrane helix bundle. This is true no matter which region of TMH5 is treated as flexible (see Figure 18).

TMH6

The helices obtained from CM calculations show that the TMH6 population leans toward the TMH5 at the extracellular end. By comparing the sequence of rhodopsin and GPR55, it can

be noted that the extracellular loop 3 (EC3) has eight extra residues in GPR55 (RNSFIVECRAKQSI) compared to Rho (QGSDFG) , thus allowing GPR55 TMH6 to lean further away from TMH7 and closer to TMH5.

TMH7

The results for TMH7 were unusable because none of the helices could fit in context of full bundle due to high bend angles. This was possible since the calculations were run in vacuum and not in the context of a bundle.

The results of these Conformational Memories calculations will be used to refine the current GPR55 model. There are other regions of the GPR55 sequence that may also diverge from the Rho structure. For example, serine and threonine residues can also bend helices. We will not pursue the hypothesis that a Ser or Thr may be altering helix conformation, however, until we have experimental mutation results that might suggest a distortion in a given helix relative to the current model. For example, in TMH3, the region SMYGS, from 3.35-3.39 and in TMH4, the region WTGSIP, from 4.54-4.59, would be possible flexible regions that could be studied in the future. TMH1 is largely pushed away from the binding pocket in Class A GPCRs. In GPR55 TMH1, the region from 1.37-1.41 (AVHIP) would be another region that likely influences the helix conformation.

REFERENCES

Ballesteros, J. A., L. Shi, et al. (2001). "Structural mimicry in G protein-coupled receptors: Implications of the high-resolution structure of rhodopsin for structure-function analysis of rhodopsin-like receptors." Mol Pharmacol **60**(1): 1-19.

Ballesteros, J. A. and H. Weinstein (1995). Integrated Methods for the Construction of Three Dimensional Models and Computational Probing of Structure Function Relations in G Protein-Coupled Receptors. Methods in Neuroscience. S. C. Sealfon. San Diego, CA, Academic Press. **25:** 366-428

Barnett-Norris, J., D. P. Hurst, et al. (2002). "Agonist alkyl tail interaction with cannabinoid CB1 receptor V6.43/I6.46 groove induces a helix 6 active conformation." Int J Quantum Chem. **88**(1): 76-86.

Begg, M., P. Pacher, et al. (2005). "Evidence for novel cannabinoid receptors." Pharmacol Ther **106**(2): 133-145.

Borhan, B., M. L. Souto, et al. (2000). "Movement of retinal along the visual transduction path." Science **288**(5474): 2209-2212.

Boyd, R. H. (1968). "Method for Calculation of the Conformation of Minimum Potential-Energy and Thermodynamic Functions of Molecules from Empirical Valence-Force Potentials - Application to the Cyclophanes " Journal of Chemical Physics **49**(6): 2574-2583.

Brooks, B. R., R. E. Bruccoleri, et al. (1983). "CHARMM: a program for macromolecular energy, minimization, and dynamics calculations." J. Comp. Chem. **4**(2): 187-217.

Brown, A. J. (2007). "Novel Cannabinoid Receptors." British Journal of Pharmacology **152**(5): 567-575.

Brown, A. J. and A. Wise (2001). Identification of modulators of GPR55 activity. GlaxoSmithKline.

Chang, G., W. C. Guida, et al. (2002). "An internal-coordinate Monte Carlo method for searching conformational space." Journal of the American Chemical Society **111**(12): 4379-4386.

Chen, S., F. Lin, et al. (2001). "Phe303 in TMVI of the Î±1B-Adrenergic Receptor Is a Key Residue Coupling TM Helical Movements to G-protein Activationâ€ " Biochemistry **41**(2): 588-596.

Chen, S., F. Lin, et al. (2002). "Mutation of a Single TMVI Residue, Phe282, in the Î²2-Adrenergic Receptor Results in Structurally Distinct Activated Receptor Conformationsâ€ " Biochemistry **41**(19): 6045-6053.

Cherezov, V., D. M. Rosenbaum, et al. (2007). "High-resolution crystal structure of an engineered human beta2-adrenergic G protein-coupled receptor." Science **318**(5854): 1258-1265.

Devane, W. A., F. A. Dysarz, 3rd, et al. (1988). "Determination and Characterization of a Cannabinoid Receptor in Rat Brain." Mol Pharmacol **34**(5): 605-613.

Devane, W. A., L. Hanus, et al. (1992). "Isolation and structure of a brain constituent that binds to the cannabinoid receptor" " Science **258**(5090): 1946-1949.

Engel, A. and D. J. Muller (2000). "Observing single biomolecules at work with the atomic force microscope." Nature Structural Biology **7**(9): 715-718.

Ferguson, D. M. and D. J. Raber (2002). "A new approach to probing conformational space with molecular mechanics: random incremental pulse search." Journal of the American Chemical Society **111**(12):

4371-4378.

Fiser, A., R. K. G. Do, et al. (2000). "Modeling of loops in protein structures." Protein Science **9**(9): 1753-1773.

Fletcher, R. and M. J. D. Powell (1963). "A rapidly convergent descent method for minimization." Computer Journal **6** (2): 163-168.

Goutopoulos, A. and A. Makriyannis (2002). "From cannabis to cannabinergics: new therapeutic opportunities." Pharmacology & Therapeutics **95**(2): 103-117.

Guarnieri, F. and H. Weinstein (1996). "Conformational Memories and the Exploration of Biologically Relevant Peptide Conformations: An Illustration for the Gonadotropin-Releasing Hormone." J. Amer. Chem. Soc. **118**: 5580-5589.

Guarnieri, F. and S. R. Wilson (1995). "Conformational Memories and a Simulated Annealing Program That Learns - Application to Ltb(4)." J. Comp. Chem. **16**(5): 648-653.

Han, M., S. O. Smith, et al. (1998). "Constitutive activation of opsin by mutation of methionine 257 on transmembrane helix 6." Biochemistry **37**(22): 8253-8261.

Han, M., S. O. Smith, et al. (1998). "Constitutive activation of opsin by mutation of methionine 257 on transmembrane helix 6." Biochemistry **37**(22): 8253-8261.

Hanson, M. A., V. Cherezov, et al. (2008). "A specific cholesterol binding site is established by the 2.8 A structure of the human beta2-adrenergic receptor." Structure **16**(6): 897-905.

Hurst, D., J. Barnett-Norris, et al. (2006). In Silico Modeling of GPR55: Creation of an Initial Model and Refinement Based Upon Sequence Divergences in TMH6 and TMH7. 16th Annual Symposium on the Cannabinoids, International Cannabinoid Research Society.

Hurst, D. P., A. Grossfield, et al. (2010). "A lipid pathway for ligand binding is necessary for a cannabinoid G protein-coupled receptor." J Biol Chem **285**(23): 17954-17964.

Jaakola, V. P., M. T. Griffith, et al. (2008). "The 2.6 angstrom crystal structure of a human A2A adenosine receptor bound to an antagonist." Science **322**(5905): 1211-1217.

Jensen, A. D., F. Guarnieri, et al. (2001). "Agonist-induced conformational changes at the cytoplasmic side of transmembrane segment 6 in the beta(2) adrenergic receptor mapped by site-selective fluorescent labeling." Journal of Biological Chemistry **276**(12): 9279-9290.

Kirkpatrick, S. G., C.D.; Vecchi, M.P (1983). "Optimization by Simulated Annealing." Science **220**: 671-670.

Li, J., P. C. Edwards, et al. (2004). "Structure of bovine rhodopsin in a trigonal crystal form." J. Mol. Biol. **343**(5): 1409-1438.

Lin, S. W. and T. P. Sakmar (1996). "Specific tryptophan UV-absorbance changes are probes of the transition of rhodopsin to its active state." Biochemistry **35**(34): 11149-11159.

Marti-Renom, M. A., A. C. Stuart, et al. (2000). "COMPARATIVE PROTEIN STRUCTURE MODELING OF GENES AND GENOMES." Annu. Rev. Biophys. Biomol. Struct. **29**(1): 291-325.

McAllister, S. D., D. P. Hurst, et al. (2004). "Structural mimicry in class A G protein-coupled receptor rotamer toggle switches - The importance of the F3.36(201)/W6.48(357) interaction in cannabinoid CB1 receptor activation." J Biol Chem **279**(46): 48024-48037.

McAllister, S. D., G. Rizvi, et al. (2003). "An aromatic microdomain at the cannabinoid CB1 receptor constitutes an agonist/inverse agonist binding region." J Med Chem **46**(24): 5139-5152.

Mechoulam, R., S. Ben-Shabat, et al. (1995). "Identification of an endogenous 2-monoglyceride, present in canine gut, that binds to cannabinoid receptors." Biochem Pharmacol **50**(1): 83-90.

Metropolis, N., W. Rosenbluth, et al. (1953). "Equation of state calculations by fast computing machines." J. Chem. Phys. **21**(6): 1087-1092.

Mohamadi, F., N. G. J. Richards, et al. (1990). "Macromodel - An Integrated Software System for Modeling Organic and Bioorganic Molecules Using Molecular Mechanics." J. Comp. Chem. **11**: 440-467.

Mulholland, A. J., G. H. Grant, et al. (1993). "Computer Modeling of Enzyme Catalyzed Reaction-Mechanisms." Protein Engineering **6**(2): 133-147.

Mulholland, A. J. and M. Karplus (1996). "Simulations of enzymic reactions." Biochemical Society Transactions **24**(1): 247-254.

Munro, S., K. L. Thomas, et al. (1993). "Molecular Characterization of a Peripheral Receptor for Cannabinoids." Nature **365**(6441): 61-65.

Nakamichi, H. and T. Okada (2006). "Crystallographic analysis of primary visual photochemistry." Angewandte Chemie-International Edition **45**(26): 4270-4273.

Nakamichi, H. and T. Okada (2006). "Local peptide movement in the photoreaction intermediate of rhodopsin." Proceedings of the National Academy of Sciences of the United States of America **103**(34): 12729-12734.

Okada, T., M. Sugihara, et al. (2004). "The retinal conformation and its environment in rhodopsin in light of a new 2.2 angstrom crystal structure." J Mol Biol **342**(2): 571-583.

Okada, T. F., Y.; Silow, M.; Navarro, J.; Landau, E.M.; Shichida, Y (2002). "Functional role of internal water molrcules in rhodopsin revealed by X-ray crystallography." Proc Natl Acad Sci U S A **99**(9): 5982-5987.

Palczewski, K., T. Kumasaka, et al. (2000). "Crystal structure of rhodopsin: A G protein-coupled receptor." Science **289**(5480): 739-745.

Park, J. H., P. Scheerer, et al. (2008). "Crystal structure of the ligand-free G-protein-coupled receptor opsin." Nature **455**(7201): 183-187.

Ponder, J. W. and D. A. Case (2003). "Force fields for protein simulations." Adv. Protein Chem. **66**: 27-85.

Prioleau, C., I. Visiers, et al. (2002). "Conserved helix 7 tyrosine acts as a multistate conformational switch in the 5HT2C receptor - Identification of a novel "locked-on" phenotype and double revertant mutations." Journal of Biological Chemistry **277**(39): 36577-36584.

Rasmussen, S. G., H. J. Choi, et al. (2007). "Crystal structure of the human beta2 adrenergic G-protein-coupled receptor." Nature **450**(7168): 383-387.

Rasmussen, S. G., H. J. Choi, et al. (2007). "Crystal structure of the human beta2 adrenergic G-protein-coupled receptor." Nature **450**(7168): 383-387.

Reggio, P. H., N. M. Nebane, et al. (2005). A CB1 Lipid Face V6.43A/I6.46A Mutation Completely Separates the Binding Pockets of SR141716A and WIN55212-2 vs. AEA , CP55940 and HU210: Implications for Ligand Entry into CB1. 2005 Symposium on the Cannabinoids, Clearwater, Florida ICRS.

Salom, D., D. T. Lodowski, et al. (2006). "Crystal structure of a photoactivated deprotonated intermediate of rhodopsin." Proc Natl Acad Sci U S A **103**(44): 16123-16128.

Scheerer, P., J. H. Park, et al. (2008). "Crystal structure of opsin in its G-protein-interacting conformation."

Nature **455**(7212): 497-502.

Schwartz, T. W., T. M. Frimurer, et al. (2006). "Molecular mechanism of 7TM receptor activation - A global toggle switch model." Annu Rev Pharmacol Toxicol **46**: 481-519.

Schwartz, T. W. and M. M. Rosenkilde (1996). "Is there a 'lock' for all agonist 'keys' in 7TM receptors?" Trends Pharmacol Sci **17**(6): 213-216.

Serrano-Vega, M. J., F. Magnani, et al. (2008). "Conformational thermostabilization of the beta 1-adrenergic receptor in a detergent-resistant form." Proc Natl Acad Sci U S A **105**(3): 877-882.

Shi, L., G. Liapakis, et al. (2002). "Beta 2 adrenergic receptor activation. Modulation of the proline kink in transmembrane 6 by a rotamer toggle switch." v **277**(43): 40989-40996.

Singh, R., D. P. Hurst, et al. (2002). "Activation of the cannabinoid CB1 receptor may involve a W6.48/F3.36 rotamer toggle switch." J Pept Res **60**(6): 357-370.

Song, Z. H. and T. I. Bonner (1996). "A lysine residue of the cannabinoid receptor is critical for receptor recognition by several agonists but not WIN55212-2." Mol Pharmacol **49**(5): 891-896.

Teller, D. C., T. Okada, et al. (2001). "Advances in determination of a high-resolution three-dimensional structure of rhodopsin, a model of G-protein-coupled receptors (GPCRs)." Biochemistry **40**(26): 7761-7772.

Thomas, G. H. (2001). "New routes to membrane protein structures - Practical course: Current methods in membrane protein research." Embo Reports **2**(3): 187-191.

Visiers, I., B. B. Braunheim, et al. (2000). "Prokink: a protocol for numerical evaluation of helix distortions by proline." Protein Eng **13**(9): 603-606.

Von Dreele, R. B. (1999). "Combined Rietveld and stereochemical restraint refinement of a protein crystal structure." Journal of Applied Crystallography **32**(6): 1084-1089.

Von Dreele, R. B., P. W. Stephens, et al. (2000). "The first protein crystal structure determined from high-resolution X-ray powder diffraction data: a variant of T3R3 human insulin-zinc complex produced by grinding." Acta Crystallographica Section D-Biological Crystallography **56**: 1549-1553.

Warne, T., M. J. Serrano-Vega, et al. (2008). "Structure of a beta1-adrenergic G-protein-coupled receptor." Nature **454**(7203): 486-491.

Weiner, S. J., P. A. Kollman, et al. (1984). "A new force field for molecular mechanical simulations of nucleic acids and proteins." Journal of American Chemical Society **106**(3): 765-774.

Whitnell, R. M., D. P. Hurst, et al. (2007). "Conformational memories with variable bond angles." Journal of Computational Chemistry **29**(5): 741-752.

Wiberg, K. B. (2002). "A Scheme for Strain Energy Minimization. Application to the Cycloalkanes1." Journal of the American Chemical Society **87**(5): 1070-1078.

Yao, X. J., C. Parnot, et al. (2006). "Coupling ligand structure to specific conformational switches in the beta(2)-adrenoceptor." Nat Chem Biol **2**(8): 417-422.

Yeagle, P. L. and A. D. Albert (2007). "G-protein coupled receptor structure." Biochimica Et Biophysica Acta-Biomembranes **1768**(4): 808-824.

Zhang, R., D. P. Hurst, et al. (2005). "Cysteine 2.59(89) in the Second Transmembrane Domain of Human Cb2 Receptor Is Accessible within the Ligand Binding Crevice: Evidence for Possible Cb2 Deviation from a Rhodopsin Template." Mol Pharmacol **68**(1): 69-83.